The climate response to stratospheric sulfate injections and implications for addressing climate emergencies

Kelly E. McCusker *, David S. Battisti, and Cecilia M. Bitz

University of Washington, Seattle, Washington

ABSTRACT

Stratospheric sulfate aerosol injection has been proposed to counteract anthropogenic greenhouse gas warming and prevent regional climate emergencies. Global warming is projected to be largest in the polar regions, where consequences to climate change could be emergent, but where the climate response to global warming is also most uncertain. We use the Community Climate System Model version 3 to evaluate simulations with combinations of enhanced CO_2 and stratospheric sulfate to investigate the effects on regional climate, and further explore the sensitivity of these regions to ocean dynamics by running a suite of simulations with and without ocean dynamics.

We find that when global average warming is roughly canceled by aerosols, temperature changes in the polar regions are still 20-50% of the changes in a warmed world. Atmospheric circulation anomalies are also not canceled, which affects the regional climate response. We also find that agreement between simulations with and without ocean dynamics is lowest in the high latitudes. The polar climate is determined by important processes that are highly parameterized in climate models. Thus, one should expect that the projected climate response to geoengineering will be as uncertain in these regions as it is to increasing greenhouse gases. In the context of climate emergencies such as melting arctic sea ice and polar ice sheets, and food crisis due to a heated tropics, we find that the potential for avoiding tropical crisis is likely, whereas avoiding the polar emergencies is not certain. We suggest a coordinated effort across modeling centers is required to generate a more robust depiction of a geoengineered climate.

1. Introduction

a. Motivation

The Intergovernmental Panel on Climate Change Fourth Assessment Report (IPCC AR4) projects global and annual mean warming of 1.7 to 4.4 °C this century under the A1B emissions scenario (Meehl et al. 2007). Warming in the northern high latitudes is projected to be 1.5 to 4.5 times the global mean values in global climate models (Holland and Bitz 2003). Even under stabilized emissions or cessation of emissions, the planet will continue to warm due to the gases that have already been emitted (Matthews and Caldeira 2008; Ramanathan and Feng 2008; Solomon et al. 2009), with a very real possibility that committed warming is equal to or greater than "dangerous" levels (Ramanathan and Feng 2008) that some claim may have catastrophic consequences (Hansen et al. 2007). Blackstock et al. (2009) define climate emergencies as "those circumstances where severe consequences of climate change occur too rapidly to be significantly averted by even immediate mitigation efforts". Such emergencies would include, for example, the loss of habitat for polar bears, displaced arctic ecosystems, thawing permafrost, rapid sea level rise due to melting Greenland and West Antarctic ice sheets, or a large reduction in crop production due to small temperature changes in the tropics.

Recent Arctic warming and record summer sea-ice area minimums have spurred expressions of concern for, and investigations into, the fate of sea-ice dependent polar bears (Regehr et al. 2010), arctic ecosystems (Grebmeier et al. 2006), permafrost (Lawrence et al. 2008), and the way of life of local communities (Hinzman et al. (2005) and references therein). Each of these systems depends on either sea-ice area (e.g., for hunting, resting, breeding; Moore and Huntington (2008)) or subfreezing surface temperatures over land (e.g., permafrost and Greenland). Maintaining surface temperatures and preserving sea-ice are thought to be necessary to avoid threatening such systems.

On the other side of the globe, the world's greatest ice sheets are found in West Antarctica and the Antarctic Peninsula, storing huge amounts of water that could potentially raise sea level by many meters. There is a very real danger that land ice calving and/or melting could accelerate and cause greater sea level rise than is anticipated from thermal expansion of seawater alone. The catalysts for such events are higher air temperatures, and more im-

portantly, warmer ocean waters sloshing up against the ice sheet outlets that melt outlet glaciers and ice shelves and could destabilize grounding lines (Oppenheimer 1998; Schoof 2007). The most in-peril ice sheets flow into the Ross and Weddell Seas (Oppenheimer 1998) in West Antarctica, which has been shown to be warming currently (Steig et al. 2009), and losing ice mass (Chen et al. 2009; Velicogna 2009).

Whereas the greatest warming is projected to occur in the polar regions, the tropics show relatively modest temperature changes under increasing CO_2. Nonetheless, ecosystems in the tropics may be among those most affected by a changing climate: small amplitude climate variability in the tropics, combined with a tightly coupled ocean-atmosphere system, means that even small climate changes can have important consequences for living systems, whose evolution was built on a narrow range of temperature. Organisms that are accustomed to stable climatic conditions have lower physiological thresholds, and thus are put under more stress for a given warming than those from more climatically variable regions (Tewksbury et al. (2008) and references therein). Moreover, plants and crops grown in the tropics, providing livelihood and sustenance to billions of people, abide by similar laws, and so even small climate changes in the tropics can be detrimental. Global warming will cause temperature and precipitation to surpass optimal growing conditions, adversely affecting ecosystems, agriculture, and food security for billions (Battisti and Naylor 2009).

Should climate evolve as models predict, and severe consequences emerge, swift action may become necessary. However, even if all anthropogenic emissions of greenhouse gases ceased, the planet would continue to warm, possibly by a significant amount (Armour and Roe 2011; Hare and Meinshausen 2006). Thus the only solution in such a scenario would be to cancel the rise in temperature by some other means. Accordingly, the domain of feasible solutions to the global warming problem has expanded from adaptation and mitigation by greenhouse gas emissions reductions to include geoengineering: the deliberate modification of the Earth's radiative budget in order to stop the climate change due to increasing anthropogenic greenhouse gases. Geoengineering has evolved from a topic of intermittent discourse between scholars (via publications), to news media and the blogosphere. Recently, major world governments and important scientific societies - such as the The Royal Society of the United Kingdom (The Royal Society 2009), the American Meteorological Society (American Meteorological Society 2009), and the U.S. Government Accountability Office - have made formal statements and issued reports on the topic. Exploration of implementation and deployment technologies, in some form or another, is currently being undertaken (Blackstock et al. 2009), even to the point of pending patent applications [1]. Our current understanding of the effect geoengineering will have on the climate system, especially on a regional scale, is not sufficient to rule out unfavorable consequences (Robock et al. 2010), however, and calls for more research have been made (American Meteorological Society 2009; Hegerl and Solomon 2009; Keith et al. 2010).

Numerous schemes have been proposed to alleviate the warming due to anthropogenic emissions of greenhouse gases. These schemes fall into two groups: those that alter the sources and sinks of carbon in the Earth system, and those that alter the albedo of the planet. Several implementation schemes have been proposed to accomplish albedo-management. These proposals include placing reflective mirrors in space, seeding clouds to make them brighter, and injection of sulfate aerosols or its precursors into the stratosphere. Each of these schemes would work by allowing less shortwave energy to reach the surface of the planet, thereby reducing surface temperature. It is unknown which of these ideas may be most effective in alleviating temperature rise. However, sulfate injection is the leading contender because it is inexpensive to implement, uses existing technology (Robock et al. 2009), and it would be quick to affect surface temperatures if commenced, as well as quick to terminate (Matthews and Caldeira 2007; Robock et al. 2008; Brovkin et al. 2009). These factors place stratospheric sulfate injections on top of the list of relatively realistic solutions that could be deployed in the near future and is the guiding reason for our choice to simulate these injections in a GCM and study its effects on the model's regional climate.

b. Background

Many of the geoengineering modeling studies to date evaluate the impact of aerosols or sunshade technology by uniformly reducing the solar constant in a model. Govindasamy and Caldeira (2000) and Govindasamy et al. (2003) showed in their studies that uniformly reducing the solar constant in an atmosphere general circulation model (AGCM) coupled to a slab ocean sufficiently canceled the global mean warming due to doubling and quadrupling CO_2, respectively. They found a greater cooling in the tropics compared to the poles and a reduction in seasonal amplitude of temperature. In the context of the polar emergencies discussed in the Section 1a, these studies suffer from the exclusion of ocean and sea-ice dynamics. Lunt et al. (2008) performed a similar study, but with an AGCM coupled to a full ocean GCM, albeit at low resolution, wherein they quadrupled CO_2 and reduced the solar constant. They noted a reduced pole-to-equator temperature gradient, reduced temperature seasonality, and a reduced

[1] Intellectual Ventures Lab, Stratoshield White Paper, http://intellectualventureslab.com/wp-content/uploads/2009/10/Stratoshield-white-paper-300dpi.pdf

intensity of hydrologic cycle compared with a pre-industrial control. Matthews and Caldeira (2007) investigated the transient response of the climate to insolation reduction in a model with an interactive carbon-cycle, made up of an energy-moisture balance atmosphere, dynamic ocean, and dynamic-thermodynamic sea ice. Their study emphasized the fast response time of the climate to turning on and off geoengineering. All of the above studies are limited for the purpose of understanding the effects of stratospheric aerosols by use of a forcing (reduced solar constant) that has a very different spatial structure than would be realized by stratospheric aerosol injections, which we will show also has important implications for the response of the climate system to the net forcing of increased carbon dioxide plus aerosols.

The combination of imposed forcings is not necessarily, a priori, expected to result in stabilized climate on a regional scale for three reasons. First, stratospheric sulfate forcing, such as is prescribed in our experiments, does not have the same properties as a forcing from increased carbon dioxide because the former primarily acts on shortwave radiation and the latter primarily on longwave radiation. Thus, due to lack of sunlight, the efficacy of sulfate aerosols in the polar regions may be diminished. Second, studies have shown that modifications to shortwave versus longwave radiation affect temperature and precipitation differently (Allen and Ingram 2002; Bala et al. 2008). A perfect cancellation of surface temperature by solar radiation management necessarily excludes perfect cancellation of precipitation, because of the differing energetic properties of the radiative forcings. Third, the spatial distribution of stratospheric sulfate aerosol versus carbon dioxide is not identical, with carbon dioxide being well-mixed in the troposphere, and a sulfate layer limited to the lower stratosphere. The latter effect, we will show, has profound implications for the response of the climate - and especially for the effectiveness of geoengineering to avoid the two polar emergencies we consider here. Even if the negating effect of a sulfate layer was perfect, there is also some question as to just how feasible it is to tune to the correct amount of sulfate in the real world, where timescales of adjustment are spatially varying and large natural variability will obscure the response of the earth system to changes in forcing.

Modeling studies of the response of the climate system to geoengineering have become more realistic by including simulation of aerosol injection into the stratosphere (Rasch et al. 2008a; Robock et al. 2008; Jones et al. 2010). Rasch et al. (2008a) simulated geoengineering by injecting sulfur dioxide into the stratosphere, in such a manner that the quantity of particles would provide enough (globally averaged) negative radiative forcing to counteract the positive radiative forcing due to a doubling of carbon dioxide. They found that the size distribution of the aerosols affected the efficacy of the cooling - specifically smaller sizes were more effective.

Robock et al. (2008) were the first to utilize a climate model with a dynamical ocean and sea-ice to investigate the transient response to geoengineering with stratospheric sulfur injections. They simulated both tropical and arctic instantaneous injections and found that the effect of arctic injections, whose purpose was to recover sea-ice extent, was not restricted to the arctic region but extended south to 30°N. Their model results also displayed a weakening of the Asian and Africa summer monsoons. Though both Rasch et al. (2008a) and Robock et al. (2008) use a more realistic forcing, in the context of the climate emergencies in the polar regions, both of these studies lack key ingredients. First, Rasch et al. (2008a) do not include sea ice or ocean dynamics and second, the sea-ice component of the model employed by Robock et al. (2008) is very insensitive to either greenhouse gases or stratospheric aerosol (Jones et al. 2010) and the ocean resolution used is extremely coarse. Ammann et al. (2010) conduct fully-coupled atmosphere-ocean model simulations that transiently counteract greenhouse warming (via the IPCC A2 scenario) with either a solar reduction or stratospheric injection of sulfur dioxide, and focus on the regional effectiveness of the combined radiative forcing. They find that the net forcing induces enhanced atmospheric zonal circulation anomalies, which contribute to residual Arctic warming.

The objective of this study is to investigate whether the climate emergencies can be avoided through solar management by injecting sulfate aerosols into the stratosphere. To our knowledge, this is one of the first attempts to maintain global mean surface temperature transiently, in a fully coupled GCM with a more realistic forcing (but see also Ammann et al. (2010)). We do this by ramping up carbon dioxide concentration concurrently with stratospheric aerosol concentration, in our case with a prescribed sulfate burden. We compare experiments performed with climate models with and without full ocean dynamics to illuminate some of the uncertainties in projecting a potential future geoengineered world that are particularly relevant to the climate emergencies. We will focus on three main regions of concern: the Arctic circle, the West Antarctic ice sheet region (including the Antarctic Peninsula), and the tropics. The paper is organized as follows. Section 2 describes the global climate model and experiment design. Results are described in Section 3. We first discuss the transient simulations and broad global results. We further consider the vertical structure of the atmospheric response to stratospheric aerosols and to increased carbon dioxide, and then discuss regional surface climate response to these forcings in the context of the three climate emergencies. We expound upon the uncertainties and discuss the broader implications of our results in Section 4. Conclusions are presented in Section 5.

2. Model and Simulations

We perform our experiments using the National Center for Atmospheric Research (NCAR) Community Climate System Model version 3 (CCSM3) (Collins et al. 2006), which has components for atmosphere, ocean, land, and sea ice. We run each simulation with T42 resolution (approximately 2.8°) in the atmosphere and a nominal 1 degree resolution in the ocean. The atmosphere has 26 vertical levels while the ocean has 40 vertical levels.

We run a suite of simulations with the atmosphere component of the CCSM3 coupled to either a slab ocean or to the full Ocean General Circulation Model (OGCM) of CCSM3 to determine the effect of ocean dynamics on the climatic response to geoengineering (see Table 1). The slab ocean utilized is a modified version of the more common slab ocean model with motionless sea ice. Our version has the complete CCSM3 thermodynamic-dynamic sea ice model, and we refer to it as the Dynamic sea Ice Slab Ocean Model (DISOM). This model was introduced and used by Holland et al. (2006) and Bitz et al. (2006). The full atmosphere-ocean general circulation model configuration of CCSM3 is called OGCM in this paper. The ocean heat flux convergence (OHFC) prescribed in the DISOM simulations is derived from the surface flux and ocean heat storage climatology of the full OGCM from a 1990's CCSM3 control so that the mean state of the DISOM and OGCM control simulations are the same. We use the ocean component (i.e., DISOM and OGCM) to differentiate the model configurations when referring to simulations (see Table 1).

We conduct experiments with various carbon dioxide concentrations, some in combination with geoengineering. We do this using both configurations of CCSM3, (i) DISOM (equilibrium) and (ii) OGCM (transient), so that we conduct a total of 8 simulations, listed in Table 1. For each model configuration we have a *control* run (annually periodic external forcing from 1990s levels, with CO_2=355ppm and other greenhouse gases set to 1990 levels), an increased CO_2 run (*co2*), a stratospheric sulfate-only run (*aero*), and a "net" run that has both increased CO_2 and a sulfate layer (*geoco2*).

The forcings are applied instantaneously in the DISOM experiments, and then we run the model to equilibrium (a minimum of 40 years). We analyze the last 40 years of the DISOM *control* and *geoco2* runs and the last 20 years of the *co2* and *aero* runs. The CCSM3 OGCM *control* and *co2* runs were obtained from NCAR (Collins et al. 2006). Carbon dioxide concentration is ramped at 1% per year from the 1990 level. We ramp the sulfate burden linearly from zero, so that the amount prescribed at any given time provides a global average negative radiative forcing that approximately equals the positive radiative forcing of the carbon dioxide. In the case of *geoco2*, we integrated the model until the carbon dioxide reached four times modern concentrations of CO_2 and the sulfate burden reached 16 teragrams of sulfur equivalent (TgS). Figure 2a depicts the years for which means are computed for each transient simulation. We have one ensemble member for the OGCM *geoco2* simulation that was not available during the initial analysis and writing of the paper. The ensemble member exhibits essentially the same global mean changes (to within 1%) and spatial pattern of response as the *geoco2* analyzed here, providing greater robustness to our conclusions.

The sulfate forcing, or imposed "geoengineered layer", is a prescribed burden of sulfate (SO_4) in the stratosphere and has a monthly climatology, repeating annually. The annually and zonally averaged mass of sulfate in the atmosphere at the time of CO_2 doubling is shown in Figure 1, which corresponds to a total annual mean burden of 8 TgS. By prescribing the aerosol distribution, we ignore a major additional source of uncertainty in our study: the chemistry of sulfate formation and its transport. However, these processes were taken into account in the generation of the SO_4 climatology. The SO_4 climatology is taken from the results of a model study by Rasch et al. (2008a), whereby they continuously injected a prescribed size distribution of SO_2 (sulfur dioxide) into the stratosphere at an altitude of 25 km from 10°N to 10°S, where it was transported by winds and interacted chemically. They used a prescribed size distribution with a dry mode radius, standard deviation, and effective radius values of 0.05, 2.03, 0.17 μm, respectively, which is meant to simulate a volcanic-like distribution. Once in the stratosphere, the SO_2 oxidizes to form sulfate aerosol, which is transported and removed via wet and dry deposition.

In the study by Rasch et al. (2008a), the volcanically-sized aerosol distribution did not fully cancel the warming due to doubled carbon dioxide. Because we prescribe the aerosol distribution, we have scaled up the sulfate climatology by the same fraction at each latitude and height in the atmosphere, to better cancel the equilibrium warming under the 2xCO_2 scenario experiment in DISOM. This results in an annual mean prescribed burden of sulfur equivalent in our simulations of 8 TgS (to counteract 2xCO_2) compared with 5.9 TgS in Rasch et al. (2008a). It has been shown that there may be some limitation to the effectiveness of sulfate aerosols when the microphysics of sulfur dioxide injection and sulfate aerosol formation are taken into account, such that the burden required to cancel a doubling of CO_2, for instance, would be greater than what is estimated in our study (Heckendorn et al. 2009), and some have suggested that directly injecting sulfuric acid vapor may improve the mass to radiative forcing ratio (Pierce et al. 2010). However, we focus our attention on the climate response induced by an aerosol layer that, in our model, achieves a radiative forcing that is approximately equal and opposite to that of doubled CO_2, which

assumes that such a layer can be deployed in reality.

3. Results

Our suite of experiments shows the extent to which global and annual mean warming from rising CO_2 can be offset by placing sulfate aerosols with particular optical properties and spatial distribution in the stratosphere. We first show global-mean, annual-mean results and annual mean spatial maps as a baseline. We then turn our focus to specific regions, namely the Arctic, West Antarctica and the Antarctic Peninsula, and the tropics, in order to examine the results in the context of climate emergencies.

a. Global

Table 2 lists globally, annual averaged values of temperature, precipitation, and sea-ice area and volume from the set of simulations. It is no surprise that the equilibrium temperature change of the DISOM *geoco2* case relative to the DISOM *control* is near zero (Table 2) because we adjusted the concentration of aerosols specified in the DISOM *geoco2* run through several iterations. It is more remarkable that the transient warming in the OGCM forced by ramping CO_2 at the rate of 1% per year, shown in Figure 2a, can be effectively canceled up to about the 70th year after forcing commencement (the time of CO_2 doubling) by linearly ramping sulfate aerosol concentration in the stratosphere.

For reference, Figures 3a and 3b show the spatial maps of annual average surface temperature change between the DISOM and OGCM *co2* and *control* simulations and Figures 3c and 3d show the companion maps for *geoco2*. In the annual mean, the presence of a sulfate aerosol layer is able to cancel surface temperature rises due to increased CO_2 nearly everywhere but the Arctic, which will be discussed in more detail in the Arctic subsection.

The OGCM exhibits a slight global mean warming at the end of the analysis period (see Figure 2a). Hence, we also compute the linear temperature trend spatially for the period before the global mean temperature diverges from the *control* (years 11-80). Figure 4 shows the magnitude of the temperature change extrapolated to year 80 (the midpoint of the analysis period) computed using the linear trend of annual mean global mean surface temperature for years 11-80. The pattern that emerges matches that seen in Figure 3d, indicating that the spatial pattern of response is fundamental to the combination of increasing CO_2 and increasing sulfate layer burden, and is not influenced by the existence of a residual global mean warming (0.08°C in the forty year average).

When aerosol concentrations are designed to cancel global warming, they do not also cancel global mean precipitation changes (Bala et al. 2008; Robock et al. 2008; Ricke et al. 2010). Indeed placing sulfate aerosols in the stratosphere reduces precipitation more than it increases on average from raising CO_2. Thus, the globally averaged precipitation rate declines by between 1 and 2% at the time of CO_2 doubling for both transient and equilibrium *geoco2* cases relative to their *controls* (see Table 2). Figure 2b shows the change in precipitation with time for the OGCM simulations. Although the globally averaged surface temperature stays nearly constant for the first 80 years of the *geoco2* experiment, precipitation slowly declines with increasing sulfate burden. This result supports the theory put forth in Allen and Ingram (2002), whereby longwave and shortwave radiation affect precipitation and temperature differently.

Figure 2c displays the top of atmosphere (TOA) net flux anomaly from the control simulation for the OGCM *co2*, *aero*, and *geoco2*. The OGCM *geoco2* has an annual mean TOA imbalance anomaly of 0.06 Wm^{-2} during our analysis period, while the DISOM *geoco2* has an imbalance of less than 0.01 Wm^{-2}, indicating that the *geoco2* simulations are well balanced and the radiative forcing from the imposed sulfate layer successfully counterbalances that from increased CO_2 during the analysis period.

b. Vertical structure

The global average forcing at the top of the atmosphere in the *geoco2* experiments is effectively zero until the time of CO_2 doubling, but there are important spatial differences, particularly in the vertical. We discuss and show the DISOM results of the vertical and zonal mean temperature in this section as an example, however the OGCM has a very similar vertical temperature response to the combined CO_2 and aerosol forcing. Raising CO_2 causes tropospheric warming and slight-to-no cooling in the lower stratosphere (Figure 5a). The sulfate aerosol concentration is at a maximum over the tropics, where the original injection of sulfur dioxide in the Rasch et al. (2008a) study was located, which causes an increase in absorption of solar and infrared radiation there compared to the control climate. By virtue of this spatial distribution, the sulfate aerosol produces a local warming maximum in the lower stratosphere over the tropical region (Figure 5b). The net result of doubled CO_2 and a sulfate layer on zonal mean temperature is to leave the troposphere much like the 1990s control (Figure 5c). Yet in the stratosphere, the cooling due to increased carbon dioxide does little to abate the tropical stratosphere sulfate-driven warming. These non-neglible changes in the vertical structure of temperature in the atmosphere cause noticeable differences to the zonal mean wind field.

Figures 5 d-f display the vertical structure changes in zonal mean zonal wind in the DISOM perturbation experiments. In the annual mean, enhanced CO_2 forces the southern hemisphere (SH) polar stratospheric vortex to shift equatorward, while the northern hemisphere (NH) polar stratospheric vortex displays a broad, weak enhancement in the upper atmosphere (Figure 5d). The subtropi-

cal tropospheric jets and zonal mean surface winds change little due to doubled CO_2. In contrast, forcing by sulfate aerosols alone causes a clear poleward shift of the stratospheric and tropospheric polar vortex in the SH and a strengthening of the stratospheric polar vortex in the NH (Figure 5e). The net result of the combined forcings in *geoco2* looks similar to that of the sum of the two separate forcings. In the NH the polar vortex is strengthened even more in *geoco2* than in *co2* (an increase in mean zonal wind of about 30% at the peak location compared to 20% in *co2*), and this strengthening is especially apparent in DJF (not shown) where the strengthening also extends down to the surface. In the SH the net result is an equatorward shift of the stratospheric polar vortex and a poleward shift in the jet in the troposphere. The zonal mean temperature and wind response patterns look very similar in the OGCM for the *geoco2* case. Thus, the addition of sulfates does not counteract the circulation anomalies due to increased CO_2. We will see in the following sections that these upper level differences are indeed manifested at the surface as changes in climate (although the surface wind response tends to be weaker in OGCM than DISOM).

c. The Arctic

Figures 6a and 6b display the change in summer (June, July, August - JJA) surface temperature in the *geoco2* simulations as compared to the *control* integrations for the DISOM and the OGCM, respectively. Also noted on the figure is the location of the sea-ice edge, defined as the region within which there is a 15% or greater sea-ice concentration, for *geoco2* (dashed) and *control* (solid). As expected, summer temperatures over sea ice remain unchanged, as ice keeps the air temperature at about 0°C in summer. However, northern land surfaces are over-cooled in both models, at some locations by over 1°C, with the notable exception of warming in Greenland. Although the sea-ice edge in the Arctic is nearly unchanged, the NH sea ice volume is reduced by 10.0% and 2.8% for DISOM and OGCM, respectively, with the greatest thinning of sea-ice focused around Greenland (not shown). Additionally, there are reductions in sea-ice concentration (not shown) of up to 10% in the marginal ice zones, especially in DISOM.

Figures 6c and 6d show the change in surface temperature, but in northern hemisphere winter (December, January, February - DJF). Contrary to JJA, the DJF surface temperature response in *geoco2* displays a consistent residual warming of 2-4°C in northern Eurasia in both model configurations. Although cooler than a 2xCO_2 world, temperatures are still up to 50% of the 2xCO_2 warming here, with the most expansive warming occurring in the DISOM model (cf Figure 3a, b with Figure 6 c, d). Yet, as in JJA, DJF sea-ice extent is nearly unchanged (see Figure 6).

Compared with the *control* climate, both the DISOM and the OGCM *geoco2* simulations have enhanced winter west-to-southwesterly winds at 950 mb over northern Eurasia and the northern Atlantic ocean and Nordic seas, with the OGCM 950 mb wind enhancement mostly limited to the Nordic seas (Figure 7). The enhanced winter 950 mb winds are an extension of the upper level enhancement to the polar vortex in winter, as described earlier. The 950 mb zonal wind changes are statistically significant everywhere the magnitude is about 1 ms^{-1} or greater. The circulation anomalies enhance the advection of climatologically warmer marine and lower latitude air to northern Europe and Asia ($-v' \cdot \nabla \bar{T}$), and help to explain the robust surface warming response over Eurasia. This pattern of atmospheric circulation change and surface warming is familiar as the post-volcanic eruption winter response, in which the climate exhibits a positive Arctic Oscillation (AO) phase due to a strengthened polar vortex (Robock 2000; Stenchikov et al. 2002; Shindell et al. 2004). However, the pattern cannot uniquely be attributed to the stratospheric aerosols in this case. In fact, in the *aero* simulations, the sulfate alone induces strengthened westerlies at the surface most strongly over northern Eurasia (not shown). This implies that much of this AO response pattern elsewhere is due to increased CO_2, as the *co2* case also exhibits surface circulation changes of the same sign as a positive AO (not shown). This suggests that the sulfate layer does not counteract CO_2-induced circulation changes; rather it nudges the circulation in the high northern latitudes in the same way as does increasing CO_2. These enhanced westerlies are responsible for the residual winter surface warming over Eurasia in both the DISOM and OGCM, and they exert a wind stress on the ocean that affects ocean circulation in the OGCM *geoco2* simulation (see Figure 8b). Note that the zonal wind stress changes exhibited in Figure 8 are comparable between the *co2* (8a) and *geoco2* (8b) simulations.

The spatial extent of polar residual winter surface warming in the OGCM simulation is much smaller than in the DISOM. In particular, the *geoco2* OGCM exhibits cooler SSTs near the United Kingdom and south of Greenland (where the DISOM does not), near regions of deep water formation. This cooling in the North Atlantic in the OGCM (which exists in the annual mean as well) can only be due to changes in ocean heat transport - the only difference between the two model configurations. In Figure 9, we show annual mean, Atlantic and Arctic Ocean zonal mean potential temperature and Atlantic meridional overturning circulation (AMOC) anomalies in the NH for the *geoco2* and *co2* OGCM simulations. The bottom of panel (b) shows the Atlantic and Arctic Ocean warming from increased CO_2, which in some places extends down past 2km. The lower portion of panel (d) shows the change in the AMOC due to increased CO_2, which is weakened everywhere. In the *geoco2* simulation, the sulfate aerosols have managed to cool the ocean everywhere (note the reduced

color scale), and particularly north of 50°N (upper portion of panel (b)). The effect of the combination of sulfates and increased CO_2 on the AMOC is slightly more complex. The AMOC is weakened poleward of 30°N and above 1 km in depth. The net result of the ocean temperature and circulation changes under geoengineering is a reduction in northward heat transport in the NH, shown in Figure 10 along with the *co2* and *aero* anomalies. Thus, in the *geoco2* scenario there is less residual warming and thinning of sea ice in the OGCM than in the DISOM model.

In summary, arctic climate changes induced by increasing CO_2 are not perfectly canceled by the injection of stratospheric sulfate aerosols, even when the global mean temperature change is fully canceled. There is a consistent warming signal over northern Europe and Asia in *geoco2* DJF in the DISOM and OGCM that is due to the enhanced near surface westerlies over Europe and Asia. Changes in the North Atlantic caused by the net forcings of sulfate aerosol and increased CO_2 are the same sign as, but weaker than, changes occurring under increased CO_2 alone. The residual surface winds give rise to circulation and heat transport changes in the ocean. As a result, the North Atlantic Ocean in the OGCM *geoco2* experiment exhibits cooler surface temperatures and thicker sea ice regionally in the neighboring Arctic than the DISOM, thus better canceling winter surface warming from increased CO_2.

d. The Antarctic

As in the Arctic, there is residual winter (JJA) warming over Antarctica from the combined sulfate aerosol and CO_2 forcing (Figure 11 a-b). Both the DISOM and the OGCM have residual warming on and around the Antarctic Peninsula, however the surface warming is much more focused along the Antarctic Peninsula in the DISOM, whereas it is widespread in the OGCM, extending eastward past the Weddell Sea and along the Antarctic shore to almost 130°E. It is these regions where we focus our analysis. The DISOM and the OGCM exhibit temperature changes of opposite sign over East Antarctica. Atmospheric circulation differences in DISOM and OGCM, and associated ocean dynamical responses in OGCM, are responsible for these differences in the surface temperature and sea ice responses between the DISOM and OGCM experiments.

The DISOM *geoco2* case has strengthened westerlies over the entire Southern Ocean (Figure 11c), which is a manifestation of the poleward shift in the subtropical jet (Figure 5f). The changes in atmospheric circulation lead to advection of climatological warm air from the north by the anomalous north-northwesterlies just west of the Peninsula in the DISOM, causing warming over the Bellingshausen Sea and the Peninsula. Additionally, the wind stress causes sea ice to be transported away from the east coast of the Peninsula into the Weddell Sea where it accumulates. This creates the pattern of thinner ice adjacent to thicker ice in Figure 11c. This thinner ice allows more heat from the ocean to be conducted through the ice to the air throughout the winter season. Then the thinner ice is advected eastward by the mean westerlies, generating the warming maximum along the east side of the Peninsula and extended warmth to the northeast.

The responses in Antarctic winter to the combined aerosol and CO_2 forcing in the OGCM model is different from that in the DISOM model in two ways. First, coupled feedbacks in the tropical Pacific cause changes in the mean state that affect the tropospheric winds in the SH via atmospheric teleconnections (also see Section 3e). Second, the subsequent changes in wind stress on the Southern Ocean force changes in the ocean circulation that greatly affect the upper ocean temperature and thus sea-ice thickness. We break the Antarctic response into two main regions, depicted in Figure 11d. Region A lies west of the Antarctic Peninsula and encompasses the Bellingshausen and Amundsen Seas. Region B lies east of the peninsula and is focused on the Weddell Sea but extends east to roughly 70°E.

The zonal surface wind and wind stress anomalies that are evident in the DISOM *geoco2* case are also found in the OGCM, but they are overwhelmed by a much larger eddy contribution in JJA. In particular, in region A an anomalous high pressure region (seen as anti-cyclonic wind stress circulation in Figure 11d) exists in SH winter. The geopotential height anomalies in the OGCM extend in the vertical, are nearly equivalent barotropic, and display a clear Rossby wave train signal emanating from the tropics (not shown). A recent study (Ding et al. 2011) has shown that such a high pressure anomaly in the Bellingshausen and Amundsen Seas is induced when tropical sea surface temperatures (SST) are prescribed in a GCM to have a warm anomaly in the central Pacific ocean in JJA. As is described in the next section, the OGCM *geoco2* case does indeed display a warm anomaly in the central Pacific, albeit small, but similar in magnitude and positioning as in the Ding et al. (2011) study (0.2-0.3°C in the OGCM compared with 0.2-0.4°C in Ding et al.). Thus, the warm anomalies over the western Antarctic seas and peninsula, and most importantly the Ross ice shelf, are due to anomalous atmospheric advection of mean temperature, and are consistent with tropical SST changes generating a Rossby wave train that reaches the shores of Antarctica.

Region B exhibits more expansive thinning of sea ice in the OGCM than in the DISOM, everywhere from 70°W to 60°E (see Figure 11 c-d). Figure 12 displays OGCM *geoco2* ocean potential temperature differences at various depths in SH winter, along with a cross-section of the zonal average ocean temperature difference within the longitude sector demarcated in the figure. North of about 60°S, there is warming at most depths as the nearly vertical isotherms have shifted southwards. South of roughly 60°S in the

Weddell Sea there is residual warming above about 200 m depth and cooling below, suggesting that there is anomalous upward heat transport in that region. In order to diagnose the source of heat near the surface that thins sea ice in the Weddell Sea, be it the atmosphere or ocean, we next examine ocean temperature and heat transport anomalies and perform an energy budget analysis.

We divide the Weddell Sea basin, defined by the markings in Figure 12b with a northern edge of 60°S, into upper layer (0-200m) and bottom layer (200-5000m) boxes. We then compute the vertical energy flux between the layers as a residual after taking into account the top surface fluxes, the horizontal fluxes, and the temperature tendency in the upper layer. The upper layer displays a positive temperature tendency, but a horizontal heat divergence and reduced top surface heat flux into the layer. Thus energy conservation demands that there is an anomalous upward flux of heat into the upper 0-200 meter layer from below. We find a value of 1.3 Wm^{-2} upward flux into the upper layer from below. The increase in upper layer heat in the Weddell in the *geoco2* OGCM simulation is due to the poleward shift in the Antarctic Circumpolar Current (ACC, not shown). This poleward shift in the ACC in the *geoco2* OGCM simulation (not shown) appears as an enhancement in zonal circulation at the northern edge of the Weddell Sea, a greater Ekman transport northward, and hence an increase in the divergence and upwelling of warmer circumpolar deep waters south of the shifted ACC. South of 55°S in the Weddell Sea, isotherms are shallower in the top 500 meters and are generally displaced southward in the *geoco2* run compared to the *control* run, at the approximate latitude of the ACC in this region (see Figure 12a). These changes are due to the increased zonal wind stress on the ocean (shown in Figure 8b) that occurs in the annual mean (but is obscured in Figure 11d because of the large eddy component that is evident in JJA). Notably, the *geoco2* zonal wind stress anomalies around Antarctica, shown in Figure 8b, are similar in magnitude and pattern to those in an increased CO_2 world (Figure 8a). Hence, as in the Arctic, CO_2-induced circulation changes are not canceled by the inclusion of sulfate aerosols.

e. The tropics and subtropics

Figure 13 displays the tropical and subtropical (30°S to 30°N) seasonal surface temperature changes in the *geoco2* simulations as compared to respective *controls* for DISOM and OGCM. Temperature changes within this region for all models and seasons are smaller than 1°C and usually less than 0.5 °C. In fact, much of the temperature change in the tropics under geoengineering, especially on land, is not significantly different from the control climate at the 95% level, as judged by the Student's t-test. However, there is a sizable cooling over the equatorial Pacific in DJF and JJA in DISOM, which has an effect on tropical precipitation.

Figure 14 shows the corresponding images for precipitation. As discussed earlier, in both the DISOM and the OGCM there is a net drying due to the combined forcing of aerosols and CO_2, although there is interesting and important spatial structure in the precipitation changes. Over the oceans, the cooled regions are usually drier regions (in general, the regions of statistically significant precipitation change coincide with regions of statistically significant temperature change). The control simulation of CCSM3 features a double Inter-Tropical Convergence Zone (ITCZ) over the Pacific Ocean: there are two branches of high precipitation straddling the dry equator (Collins et al. 2006) and both our DISOM and OGCM *control* simulations display this behavior. Thus the changes in precipitation in *geoco2* in the DISOM translate to a widening and strengthening of the dry tongue along the equator. It is noteworthy that the sign of the precipitation change along the equator in the central tropical Pacific in the OGCM, although not statistically significant, is opposite to DISOM, in JJA and particularly in DJF. The local precipitation maximum here is consistent with the local warming signal in the same location. This feature also appears as a local warming maximum in the *co2* runs (not shown). As discussed in the previous section, this feature in OGCM *geoco2* is associated with the generation of a teleconnection pattern in the southern Pacific Ocean in JJA that produces the anomalous high pressure west of the Antarctic Peninsula and thus the residual warming seen in the Ross and Amundsen Sea regions due to anomalous atmospheric temperature advection (see Figure 11b and d). Ocean dynamics is clearly very important to the response of the tropical pacific SST and precipitation over the ocean.

In terms of monsoonal precipitation, the DISOM and OGCM model results in Figure 14 clearly indicate an increase in summer precipitation over western India. East Asian coastal locations show a decrease in summer precipitation, and there are hints of an African summer monsoon reduction as well. However, the results are not significant in these regions. This pattern of precipitation response differs from Robock et al. (2008), which has a weakened southeast Asian monsoon, and no increase in Indian summer precipitation. In fact, across published sulfate injection studies, there is little agreement in the regional pattern of precipitation changes (Robock et al. 2008; Rasch et al. 2008b; Jones et al. 2010).

f. Beyond a 2xCO_2 geoengineered world

We extended the OGCM *geoco2* simulation past the point of CO_2 doubling to investigate whether the sulfate layer is still able to counteract increased CO_2 at higher levels. Starting from doubled CO_2 in the *geoco2* run, CO_2 is increased 1% per year and the annual mean sulfate burden is linearly increased until the concentration of CO_2 is four times 1990 levels and the aerosol burden is 16 TgS. The

green line in Figure 2a displays the timeseries of global-mean, annual-mean surface temperature. Beyond the time of CO_2 doubling (year 80 in Figure 2), the effectiveness of the aerosol to cancel the warming decreases: the global average temperature increases by 0.3°C by the time CO_2 triples and by 0.6°C by the time it quadruples. Also, by 3xCO_2, the precipitation has declined 1.8% and at 4xCO_2, 2.2%. Not surprisingly, the top of the atmosphere (TOA) radiative balance slowly becomes more positive as well. Enhanced albedo feedbacks could play a role, as there are slight reductions in surface albedo and cloud cover in the *geoco2* (not shown), but these decreases do not display stronger rates of reduction after year 80. The increasing net TOA flux is thus likely due to a slow saturation in sulfate scattering and the appearance of non-linearities in the burden to radiative forcing ratio at high sulfate burdens.

The studies of Matthews and Caldeira (2007), Robock et al. (2008), and Jones et al. (2010) indicate that the response time of the global mean surface temperature to solar management is relatively fast, and an abrupt termination of aerosol injections would cause a rapid rise in temperature back to where it would have been had no geoengineering been implemented. We performed one additional simulation where the sulfate layer was abruptly shut off at the time of CO_2 tripling, to confirm previous work investigating the effects of a sudden termination of sulfate loading. The orange line in Figure 2a indicates that a sudden termination of geoengineering leads to a rapid temperature rise back to what it would have been had such measures never been performed. In this case, the rough estimate is that the global mean temperature would rise 2°C in a matter of twenty years. Hence, the rate of temperature rise is greatly increased when compared to a scenario that never implements geoengineering.

4. Discussion

Our results show that climate change under stratospheric aerosols and increased carbon dioxide is smaller than under increased CO_2 alone. However, maintaining the modern climate is not possible: the combined forcings result in residual changes in the annual averaged climate, in the seasonality of temperature and precipitation, and in regional patterns of atmosphere and ocean circulation. Many of these residual differences result because the aerosol layer is not able to counterbalance the circulation anomalies induced under increased CO_2. Moreover, avoiding polar climate emergencies is not a certainty.

We evaluated the role of ocean dynamics by comparing experiments with a climate model coupled to a full ocean general circulation model and to a slab ocean. Under the joint forcing of increased carbon dioxide and an aerosol layer, surface temperature in northern Eurasia is cooled in summer, yet exhibits residual warming in winter. The residual climate changes in the Arctic are partially muted by ocean dynamical feedbacks that reduce the amount of poleward ocean heat transport into the North Atlantic Ocean, limiting the thinning of sea ice around Greenland and keeping SSTs cooler than when the ocean dynamics is prescribed. The repercussions of increased winter surface temperature in northern Eurasia go beyond reduced sea ice. Arctic marine mammals in general are not equipped to adapt swiftly to climate changes (Moore and Huntington 2008) and thus their well-being may be compromised by such a residual warming.

With forcing by both increased CO_2 and sulfate aerosols, Antarctica exhibits overcooling on the continent in summer (not shown) and residual warming on and around land surfaces in winter. Surface wind changes drive changes in ocean circulation and act to amplify the surface warming in winter around Antarctica. Anomalous upward ocean heat flux in the Weddell region results in slightly greater upper ocean temperatures as well. This residual upper ocean and surface air warming in and around the ice sheet exit regions does nothing to allay the potential for the West Antarctic ice sheets to become unstable due to increased melting, especially at the base of the ice shelves (Oppenheimer 1998; Meehl et al. 2007; Thoma et al. 2008; Jenkins et al. 2010). It is this instability (tipping point) that causes concern about rapid sea level rise (Notz 2009).

We find the highest effectiveness of geoengineering for our climate emergencies is in the tropics. Except in some places over the ocean, the temperature and precipitation differences under increased carbon dioxide and a sulfate layer are small. This suggests that it may be possible to avoid serious food security problems and deleterious impacts on tropical organisms, so long as the changes in surface shortwave flux do not cause adverse impacts on crop yields. Furthermore, models tend to agree more in projections of future warming in the tropical regions (see Figure 15b), providing some confidence that these tropical projections of surface temperature would be robust to the choice of model used to evaluate the impact of a geoengineering scenario. However, the inclusion of ocean dynamics is crucial, as even the sign of the equatorial Pacific Ocean temperature and precipitation response to increased CO_2 and sulfate burden depends on ocean dynamics. This affects the circulation response in the SH through teleconnections, which greatly affect the surface air and ocean temperatures that bathe the ice shelves of West Antarctica and the Antarctic Peninsula (Ding et al. 2011).

There is considerable uncertainty in other aspects of stratospheric aerosol injections that are not related to climate response, per se; for instance, the creation of the sulfate aerosol layer itself. Heckendorn et al. (2009) have found that when using a 3D chemistry-climate model with a 2D aerosol model to simulate sulfur dioxide injection into the stratosphere, the aerosol sizes grow larger than

expected. The result is an increase in particle sedimentation and an ensuing non-linear relationship between aerosol burden and injection rate, resulting in even more aerosol being necessary to stabilize the global average temperature. Others have found that increasing sulfate burden in the stratosphere could delay the recovery of the ozone hole by between 30 and 70 years due to the increased surface area the sulfate aerosol provides to catalyze ozone destruction reactions (Tilmes et al. 2008).

Model uncertainties are amplified in the sensitive high latitudes (Randall et al. 2007; DeWeaver 2007). These uncertainties result in large differences in ocean and ice variables among the IPCC AR4 models forced with a business-as-usual greenhouse gas ramping scenario (Meehl et al. 2007), and contribute to the larger spread in polar climates among Coupled Model Intercomparison Project 2 (CMIP2), which are due to wide ranges of ocean heat transport, mean state of sea ice, and cloud cover variables (Holland and Bitz 2003; Holland et al. 2001; Bitz 2008). Figure 15a displays the inter-model average of the annual-average surface temperature difference between years 2080-2099 compared to years 1980-1999 in the IPCC A1B emissions scenario among AR4 models, while Figure 15b displays the standard deviation in the ensemble average change in annual average surface temperature. The greatest differences in the projected warming are found in the Arctic Ocean and the Southern Ocean, particularly in the Ross and Weddell Seas under areas of current sea-ice cover. These are the particular regions that may experience a climate emergency.

Thus, putting our geoengineering simulations in the context of the surface temperature spread in IPCC AR4 models, it is likely that the projected polar responses to geoengineering will be highly sensitive to the choice of the climate model. Accordingly, we endorse a call, put forth by Kravitz et al. (2011), for modeling centers to unite and execute a suite of coordinated, IPCC-style geoengineering simulations in order to sort out robust and non-robust responses to geoengineering. However, as climate models fail to sample the long, low-probability tail of very high future warming that is ubiquitous in estimates of climate sensitivity (Randall et al. 2007; Knutti and Hegerl 2008; Roe and Baker 2007), they may also fail to sample the full response to geoengineering.

5. Conclusions

This study fills a gap in research on stratospheric aerosol injections by (1) imposing more realistic forcing scenarios, (2) executing geoengineering simulations using a standard resolution fully-coupled atmosphere-ocean-sea ice model with state-of-the-art sea-ice physics, and (3) comparing the result with a mixed-layer ocean model with thermodynamic-dynamic sea ice to illuminate the role of ocean dynamics. Importantly, we have also focused on regions that have the potential to experience a climate emergency. We have executed a suite of experiments to simulate stratospheric aerosol injections in a high CO_2 world (assuming that the delivery system will deliver sulfate aerosols with specified optical properties). In general, and in keeping with previous modeling work, the climatic effects of an aerosol layer plus doubled carbon dioxide are smaller than in a world with only doubled carbon dioxide. We have shown, however, that on seasonal timescales and regional spatial scales, stratospheric sulfate does not necessarily cancel all the effects of increased CO_2, especially circulation. In particular, there are still substantial climate changes in the very regions where climate emergencies may drive societies to geoengineer. Unfortunately, these are also the regions that suffer the greatest uncertainty in the response to forcing, due to strong coupling between the atmosphere, ocean, and sea ice and to deficiencies in the parameterizations of unresolved physics in the models (in particular, ocean mixing, sea ice rheology, atmospheric boundary layer processes, and clouds). Thus, one cannot rule out the possibility of geoengineering failing to avoid polar climate emergencies.

Countless other issues abound, both climatic and non-climatic, including the ignorance of other consequences of increased carbon dioxide, such as ocean acidification. The likelihood of a climate surprise occurring due to geoengineering is high because research into geoengineering is still nascent, unintended consequences are a certainty, and the uncertainties of geoengineering are layered on top of those of global warming, compounding them. The question remains as to whether the apparent global warming abatement geoengineering may provide outweighs the (i.) risk of foreseen consequences being worse than predicted (ii.) risk of altogether unforeseen negative consequences (iii.) risk of failure in international cooperation (iv.) risk of failure of the chosen geoengineering mechanisms, leading to rapid temperature rise and (v.) risk of choosing winners and losers in the climate battle. It is our opinion that it would be imprudent to believe that the risk of unintended consequences is small enough to consider geoengineering a solution at this time. More research is required, and a coordinated modeling effort is a logical first step.

Acknowledgments.

This research was funded by the Tamaki Foundation and supported in part by the National Science Foundation through TeraGrid resources provided by the Texas Advanced Computing Center under grant number [TG-ATM090059]. We would like to thank Philip J. Rasch for providing data and for thoughtful discussions on experiment design and results, Kyle C. Armour for useful comments on the manuscript, and Alan Robock and an anonymous reviewer for suggestions that improved the paper.

REFERENCES

Allen, M. R. and W. J. Ingram, 2002: Constraints on future changes in climate and the hydrologic cycle. *Nature*, **419 (6903)**, 224–232, 10.1038/nature01092.

American Meteorological Society, 2009: Geoengineering the Climate System, A Policy Statement of the American Meteorological Society. American Meteorological Society, Boston, MA.

Ammann, C. M., W. M. Washington, G. A. Meehl, L. Buja, and H. Teng, 2010: Climate engineering through artificial enhancement of natural forcings: Magnitudes and implied consequences. *J. Geophys. Res.*, **115 (D22)**, D22 109, doi:10.1029/2009JD012878.

Armour, K. C. and G. H. Roe, 2011: Climate commitment in an uncertain world. *Geophys. Res. Lett.*, **38 (1)**, L01 707, doi:10.1029/2010GL045850.

Bala, G., P. B. Duffy, and K. E. Taylor, 2008: Impact of geoengineering schemes on the global hydrological cycle. *Proceedings of the National Academy of Sciences*, **105 (22)**, 7664–7669.

Battisti, D. S. and R. L. Naylor, 2009: Historical Warnings of Future Food Insecurity with Unprecedented Seasonal Heat. *Science*, **323 (5911)**, 240–244.

Bitz, C., 2008: Some aspects of uncertainty in predicting sea ice thinning. *Geophysical Monograph*, **180**, 63–76.

Bitz, C. M., P. R. Gent, R. A. Woodgate, M. M. Holland, and R. Lindsay, 2006: The influence of sea ice on ocean heat uptake in response to increasing CO2. *Journal of Climate*, **19 (11)**, 2437–2450.

Blackstock, J. J., et al., 2009: Climate Engineering Responses to Climate Emergencies.

Brovkin, V., V. Petoukhov, M. Claussen, E. Bauer, D. Archer, and C. Jaeger, 2009: Geoengineering climate by stratospheric sulfur injections: Earth system vulnerability to technological failure. *Climatic Change*, **92 (3)**, 243–259.

Chen, J. L., C. R. Wilson, D. Blankenship, and B. D. Tapley, 2009: Accelerated Antarctic ice loss from satellite gravity measurements. *Nature Geosci*, **2 (12)**, 859–862, 10.1038/ngeo694.

Collins, W. D., et al., 2006: The Community Climate System Model Version 3 (CCSM3). *Journal of Climate*, **19 (11)**, 2122–2143.

DeWeaver, E., 2007: Uncertainty in Climate Model Projections of Arctic Sea Ice Decline: An Evaluation Relevant to Polar Bears. USGS.

Ding, Q., E. J. Steig, D. S. Battisti, and M. Küttel, 2011: Winter warming in West Antarctica caused by central tropical Pacific warming. *Nature Geosci*, **4 (6)**, 398–403, 10.1038/ngeo1129.

Govindasamy, B. and K. Caldeira, 2000: Geoengineering Earths Radiation Balance to Mitigate CO2-Induced Climate Change. *Geophys. Res. Lett.*, **27 (14)**, 2141–2144, doi:10.1029/1999GL006086.

Govindasamy, B., K. Caldeira, and P. B. Duffy, 2003: Geoengineering Earth's radiation balance to mitigate climate change from a quadrupling of CO2. *Global and Planetary Change*, **37 (1-2)**, 157–168.

Grebmeier, J. M., et al., 2006: A Major Ecosystem Shift in the Northern Bering Sea. *Science*, **311 (5766)**, 1461–1464.

Hansen, J., et al., 2007: Dangerous human-made interference with climate: a GISS modelE study. *Atmospheric Chemistry and Physics*, **7**, 2287–2312.

Hare, B. and M. Meinshausen, 2006: How Much Warming are We Committed to and How Much can be Avoided? *Climatic Change*, **75 (1)**, 111–149.

Heckendorn, P., D. Weisenstein, S. Fueglistaler, B. Luo, E. Rozanov, M. Schraner, L. Thomason, and T. Peter, 2009: The impact of geoengineering aerosols on stratospheric temperature and ozone. *Environmental Research Letters*, **4 (4)**, 045 108.

Hegerl, G. C. and S. Solomon, 2009: Risks of Climate Engineering. *Science*, **325 (5943)**, 955–956.

Hinzman, L., et al., 2005: Evidence and Implications of Recent Climate Change in Northern Alaska and Other Arctic Regions. *Climatic Change*, **72 (3)**, 251–298.

Holland, M. M. and C. M. Bitz, 2003: Polar amplification of climate change in coupled models. *Climate Dynamics*, **21 (3)**, 221–232.

Holland, M. M., C. M. Bitz, E. C. Hunke, W. H. Lipscomb, and J. L. Schramm, 2006: Influence of the Sea Ice Thickness Distribution on Polar Climate in CCSM3. *Journal of Climate*, **19 (11)**, 2398–2414.

Holland, M. M., C. M. Bitz, and A. J. Weaver, 2001: The influence of sea ice physics on simulations of climate change. *J. Geophys. Res.*, **106 (C9)**, 19 639–19 655, doi:10.1029/2000JC000651.

Jenkins, A., P. Dutrieux, S. S. Jacobs, S. D. McPhail, J. R. Perrett, A. T. Webb, and D. White, 2010: Observations beneath Pine Island Glacier in West Antarctica and implications for its retreat. *Nature Geosci*, **3 (7)**, 468–472, 10.1038/ngeo890.

Jones, A., J. Haywood, O. Boucher, B. Kravitz, and A. Robock, 2010: Geoengineering by stratospheric SO2 injection: results from the Met Office HadGEM2 climate model and comparison with the Goddard Institute for Space Studies ModelE. *Atmos. Chem. Phys. Discuss.*, **10 (3)**, 7421–7434, aCPD.

Keith, D. W., E. Parson, and M. G. Morgan, 2010: Research on global sun block needed now. *Nature*, **463 (7280)**, 426–427, 10.1038/463426a.

Knutti, R. and G. C. Hegerl, 2008: The equilibrium sensitivity of the Earth's temperature to radiation changes. *Nature Geosci*, **1 (11)**, 735–743, 10.1038/ngeo337.

Kravitz, B., A. Robock, O. Boucher, H. Schmidt, K. E. Taylor, G. Stenchikov, and M. Schulz, 2011: The Geoengineering Model Intercomparison Project (GeoMIP). *Atmospheric Science Letters*, **12**, 162–167, doi:10.1002/asl.316.

Lawrence, D. M., A. G. Slater, R. A. Tomas, M. M. Holland, and C. Deser, 2008: Accelerated Arctic land warming and permafrost degradation during rapid sea ice loss. *Geophys. Res. Lett.*, **35 (11)**, L11 506, doi:10.1029/2008GL033985.

Lunt, D. J., A. Ridgwell, P. J. Valdes, and A. Seale, 2008: Sunshade World: A fully coupled GCM evaluation of the climatic impacts of geoengineering. *Geophys. Res. Lett.*, **35**, L12 710, doi:10.1029/2008GL033674.

Matthews, H. D. and K. Caldeira, 2007: Transient climate-carbon simulations of planetary geoengineering. *Proceedings of the National Academy of Sciences*, **104 (24)**, 9949–9954.

Matthews, H. D. and K. Caldeira, 2008: Stabilizing climate requires near-zero emissions. *Geophys. Res. Lett.*, **35 (4)**, L04 705, doi:10.1029/2007GL032388.

Meehl, G., et al., 2007: *Climate Change 2007: The Physical Science Basis. Contribution of Working Group I to the Fourth Assessment Report of the Intergovernmental Panel on Climate Change*, chap. Global Climate Projections. Cambridge University Press, Cambridge, United Kingdom and New York, NY, USA.

Moore, S. E. and H. P. Huntington, 2008: Arctic marine mammals and climate change: impacts and resilience. *Ecological Applications*, **18 (sp2)**, S157–S165.

Notz, D., 2009: The future of ice sheets and sea ice: Between reversible retreat and unstoppable loss. *Proceedings of the National Academy of Sciences*, **106 (49)**, 20 590–20 595.

Oppenheimer, M., 1998: Global warming and the stability of the West Antarctic Ice Sheet. *Nature*, **393 (6683)**, 325–332, 10.1038/30661.

Pierce, J. R., D. K. Weisenstein, P. Heckendorn, T. Peter, and D. W. Keith, 2010: Efficient formation of stratospheric aerosol for climate engineering by emission of condensible vapor from aircraft. *Geophys. Res. Lett.*, **37 (18)**, L18 805, doi:10.1029/2010GL043975.

Ramanathan, V. and Y. Feng, 2008: On avoiding dangerous anthropogenic interference with the climate system: Formidable challenges ahead. *Proceedings of the National Academy of Sciences*, **105 (38)**, 14 245–14 250.

Randall, D., et al., 2007: *Climate Change 2007: The Physical Science Basis. Contribution of Working Group I to the Fourth Assessment Report of the Intergovernmental Panel on Climate Change*, chap. Climate Models and Their Evaluation. Cambridge University Press, Cambridge, United Kingdom and New York, NY, USA.

Rasch, P. J., P. J. Crutzen, and D. B. Coleman, 2008a: Exploring the geoengineering of climate using stratospheric sulfate aerosols: The role of particle size. *Geophys. Res. Lett.*, **35**, L02 809, doi:10.1029/2007GL032179.

Rasch, P. J., S. Tilmes, R. P. Turco, A. Robock, L. Oman, C.-C. Chen, G. L. Stenchikov, and R. R. Garcia, 2008b: An overview of geoengineering of climate using stratospheric sulphate aerosols. *Philosophical Transactions of the Royal Society A: Mathematical, Physical and Engineering Sciences*, **366 (1882)**, 4007–4037, doi:10.1098/rsta.2008.0131.

Regehr, E. V., C. M. Hunter, H. Caswell, S. C. Amstrup, and I. Stirling, 2010: Survival and breeding of polar bears in the southern Beaufort Sea in relation to sea ice. *Journal of Animal Ecology*, **79 (1)**, 117–127.

Ricke, K. L., M. G. Morgan, and M. R. Allen, 2010: Regional climate response to solar-radiation management. *Nature Geosci*, **3 (8)**, 537–541, 10.1038/ngeo915.

Robock, A., 2000: Volcanic Eruptions and Climate. *Rev. Geophys.*, **38**, 191-219.

Robock, A., M. Bunzl, B. Kravitz, and G. L. Stenchikov, 2010: A Test for Geoengineering? *Science*, **327 (5965)**, 530–531.

Robock, A., A. Marquardt, B. Kravitz, and G. Stenchikov, 2009: Benefits, risks, and costs of stratospheric geoengineering. *Geophys. Res. Lett.*, **36 (19)**, L19 703, doi:10.1029/2009GL039209.

Robock, A., L. Oman, and G. L. Stenchikov, 2008: Regional climate responses to geoengineering with tropical and Arctic SO2 injections. *J. Geophys. Res.*, **113**, D16 101, doi:10.1029/2008JD010050.

Roe, G. H. and M. B. Baker, 2007: Why Is Climate Sensitivity So Unpredictable? *Science*, **318 (5850)**, 629–632.

Schoof, C., 2007: Ice sheet grounding line dynamics: Steady states, stability, and hysteresis. *J. Geophys. Res.*, **112 (F3)**, F03S28, doi:10.1029/2006JF000664.

Shindell, D. T., G. A. Schmidt, M. E. Mann, and G. Faluvegi, 2004: Dynamic winter climate response to large tropical volcanic eruptions since 1600. *J. Geophys. Res.*, **109**, D05 104, doi:10.1029/2003JD004151.

Solomon, S., G.-K. Plattner, R. Knutti, and P. Friedlingstein, 2009: Irreversible climate change due to carbon dioxide emissions. *Proceedings of the National Academy of Sciences*, **106 (6)**, 1704–1709.

Steig, E. J., D. P. Schneider, S. D. Rutherford, M. E. Mann, J. C. Comiso, and D. T. Shindell, 2009: Warming of the Antarctic ice-sheet surface since the 1957 International Geophysical Year. *Nature*, **457 (7228)**, 459–462, 10.1038/nature07669.

Stenchikov, G., A. Robock, V. Ramaswamy, M. D. Schwarzkopf, K. Hamilton, and S. Ramachandran, 2002: Arctic Oscillation response to the 1991 Mount Pinatubo eruption: Effects of volcanic aerosols and ozone depletion. *J. Geophys. Res.*, **107 (D24)**, 4803, doi:10.1029/2002JD002090.

Tewksbury, J. J., R. B. Huey, and C. A. Deutsch, 2008: ECOLOGY: Putting the Heat on Tropical Animals. *Science*, **320 (5881)**, 1296–1297.

The Royal Society, 2009: Geoengineering the climate: science, governance, and uncertainty. The Royal Society, London, UK.

Thoma, M., A. Jenkins, D. Holland, and S. Jacobs, 2008: Modelling Circumpolar Deep Water intrusions on the Amundsen Sea continental shelf, Antarctica. *Geophys. Res. Lett.*, **35 (18)**, L18 602, doi:10.1029/2008GL034939.

Tilmes, S., R. Muller, and R. Salawitch, 2008: The Sensitivity of Polar Ozone Depletion to Proposed Geoengineering Schemes. *Science*, **320 (5880)**, 1201–1204.

Velicogna, I., 2009: Increasing rates of ice mass loss from the Greenland and Antarctic ice sheets revealed by GRACE. *Geophys. Res. Lett.*, **36 (19)**, L19 503, doi:10.1029/2009GL040222.

TABLE 1. Experiment Details. The run names can be understood in this way: *control* is the control run, *aero* has a prescribed sulfate layer that is annually periodic in DISOM and ramped in OGCM, and *co2* carbon dioxide doubled in DISOM and ramped in OGCM. DISOM is the Dynamic sea Ice Slab Ocean Model and OGCM has both dynamic sea ice and ocean. Columns specify the experiment name, type of ocean component, carbon dioxide concentration, and annual mean total atmospheric burden of sulfate, in units of teragrams (10^{12}g) of sulfur equivalent. The value of 1xCO_2 is 355 ppm.

Experiment	Ocean type	CO_2 Conc	Sulfate aerosol burden [TgS]
control	DISOM	1xCO_2	0
aero		1xCO_2	8
co2		2xCO_2	0
geoco2		2xCO_2	8
control	OGCM	1xCO_2	0
aero		1xCO_2	Linear ramp from 0
co2		1% Ramp from 1990 conc	0
geoco2		1% Ramp from 1990 conc	Linear ramp from 0

TABLE 2. Global annual-mean values (top) and differences (bottom) from respective control runs. OGCM means are calculated for the 40 years surrounding the time of CO_2 doubling in the *control* and *geoco2* runs. The OGCM *co2* and *aero* cases are 20 year means surrounding the time of CO_2 doubling. Surface temperature [K], precipitation rate [mm/day], total northern hemisphere (NH) sea-ice area, and total southern hemisphere (SH) sea-ice area [$10^{13}m^2$], total NH sea-ice volume, total SH sea-ice volume [$10^{13}m^3$].

Model	Exp	Sfc Temp	Precip	SIA NH, SH	SIVol NH, SH
DISOM	control	288.1	2.80	1.11, 1.23	2.75, 2.07
OGCM	control	288.0	2.79	1.12, 1.37	2.74, 2.45
		△Sfc Temp	%△ Precip	%△ SIA NH, SH	%△ SIVol NH, SH
DISOM	geoco2	0.09	-1.47	-3.89, -0.10	-9.59, 1.98
OGCM	geoco2	0.08	-1.43	-2.17, -2.21	-3.12, -3.09
DISOM	aero	-3.36	-8.54	25.5, 135	128.6, 123.6
OGCM	aero	-1.27	-3.70	15.4, -0.19	65.9, 3.03
DISOM	co2	2.70	5.21	-28.8, -45.3	-52.0, -22.4
OGCM	co2	1.38	2.15	-25.8, -10.3	-57.3, -15.7

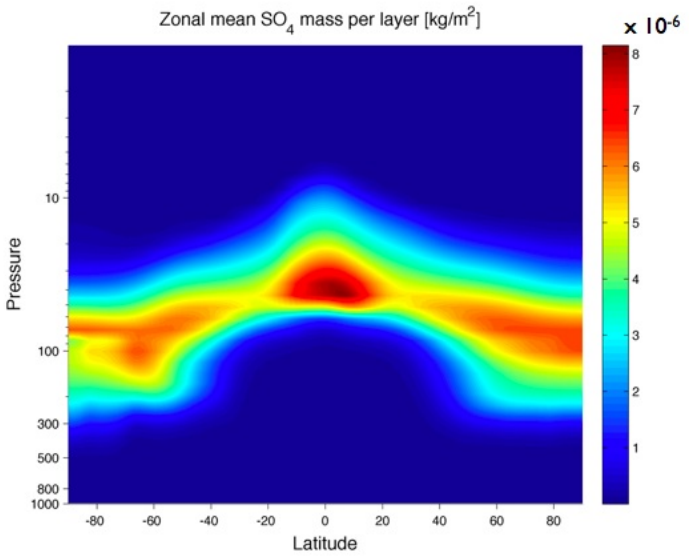

FIG. 1. The annual mean, zonal mean mass of Sulfate [kg/m^2] at 2xCO_2. The corresponding global total burden is 8 TgS.

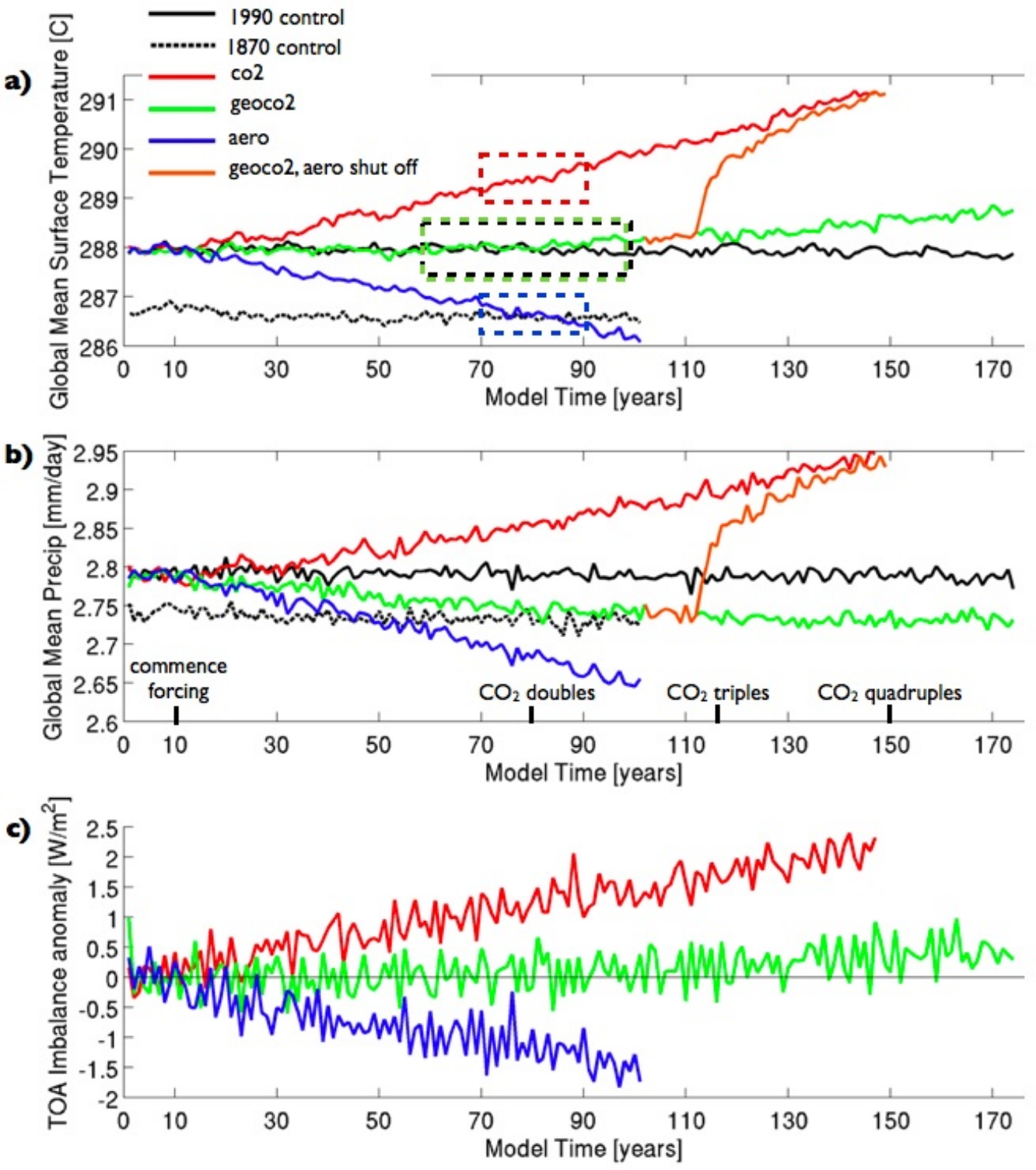

FIG. 2. Timeseries of global-mean annual-mean (a) surface temperature (°C), (b) precipitation (mm/day), and (c) top of atmosphere (TOA) radiative imbalance (W/m^2) for OGCM experiments. Ramping of sulfate and/or carbon dioxide begins in year 10 in the figure. The 1870's pre-industrial control is included for reference (black, dashed line). The boxes indicate the years of averaging for all results, unless stated otherwise in the text. Red and Blue dashed: 70-89, Black and Green dashed: 60-99.

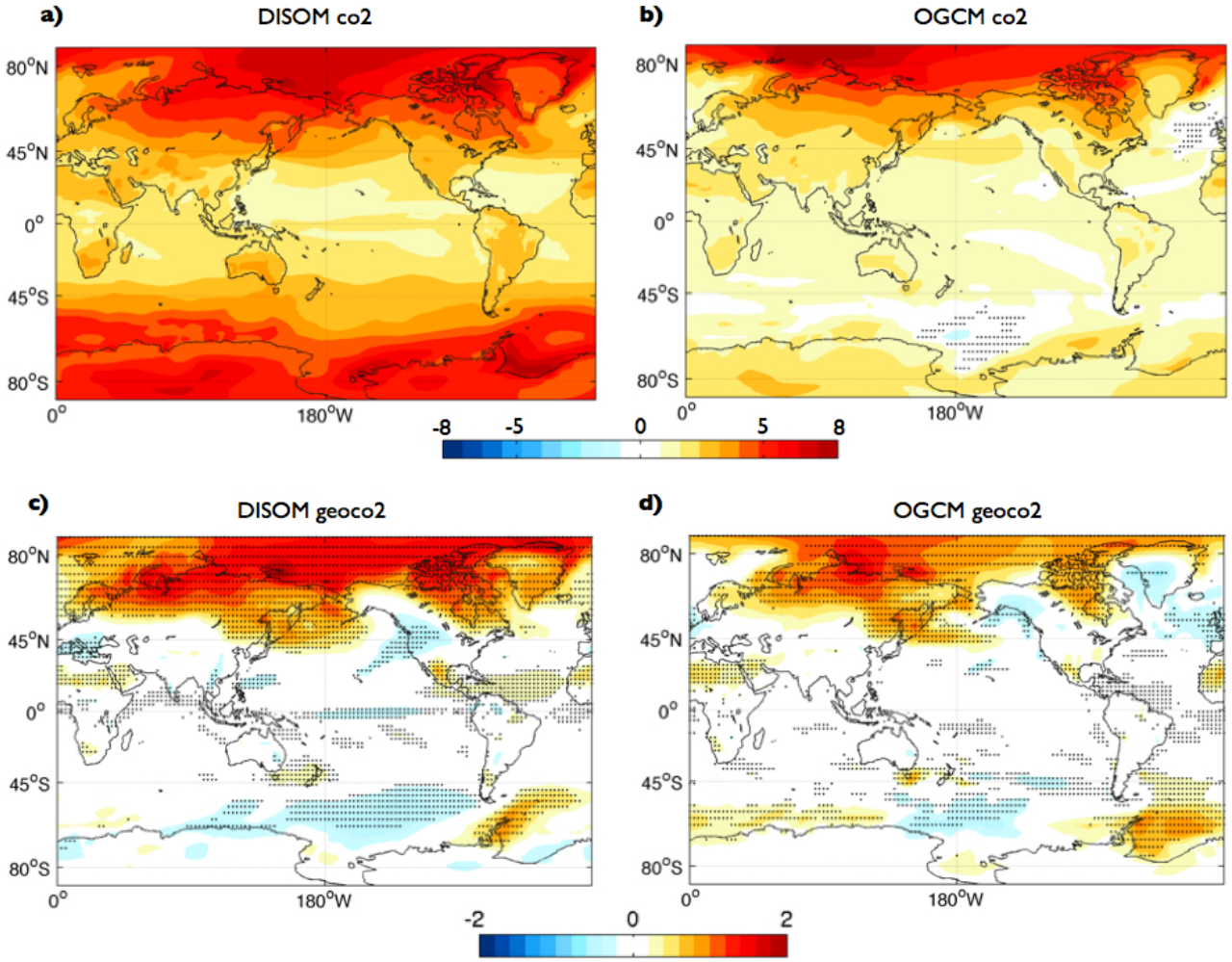

FIG. 3. Annual mean surface temperature (°C) difference between *co2* and *control* (a-b) and *geoco2* and *control* (c-d) for DISOM (at equilibrium) (a, c) and OGCM simulations (at time of CO_2 doubling) (b, d). In (a-b), the dots indicate regions of significant cooling at the 95% level, based on the Student's t-test. In (c-d), the dots indictate regions where there is significant warming or cooling at the 95% level.

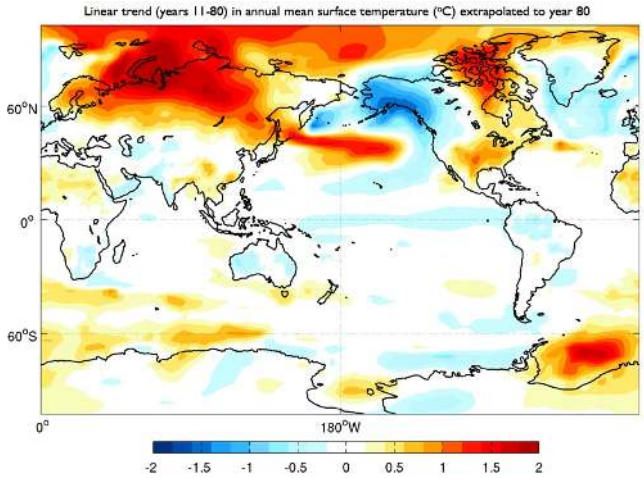

FIG. 4. Linear trend in the OGCM *geoco2* simulation for years 11-80 (before global mean surface temperature diverges from the *control*) at year 80, the midpoint of our analysis period. This shows the pattern and amplitude of warming expected at year 80, given the trend computed in years when there is no global mean surface temperature trend. The pattern and amplitude are similar to the annual mean change in temperature between the OGCM *geoco2* and *control* shown in Figure 3d. Thus, the pattern of response is fundamental to the combination of the sulfate layer and increased CO_2, not to the weakening sulfate effect at the end of the OGCM *geoco2* analysis period.

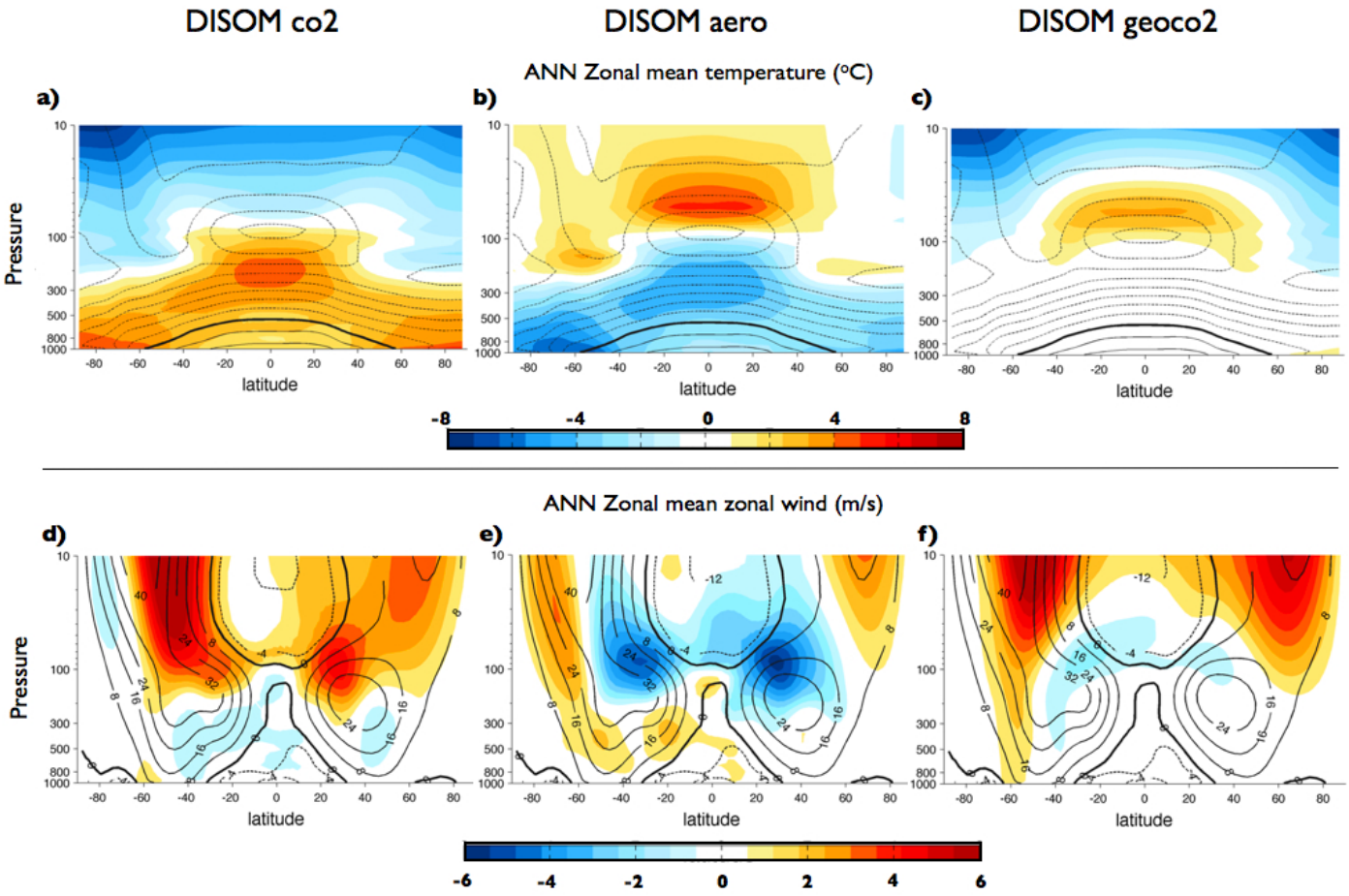

FIG. 5. Zonal-mean, annual-mean temperature (a-c) and wind (d-f) in the DISOM simulations. Contours are the *control*, in colors are differences between the perturbed experiment and the control experiment. The thick, black line indicates the zero line, dashed is negative temperature or easterly wind anomaly and solid is positive temperature or westerly wind anomaly, and the contour interval is 1.0 °C or 8 m/s.

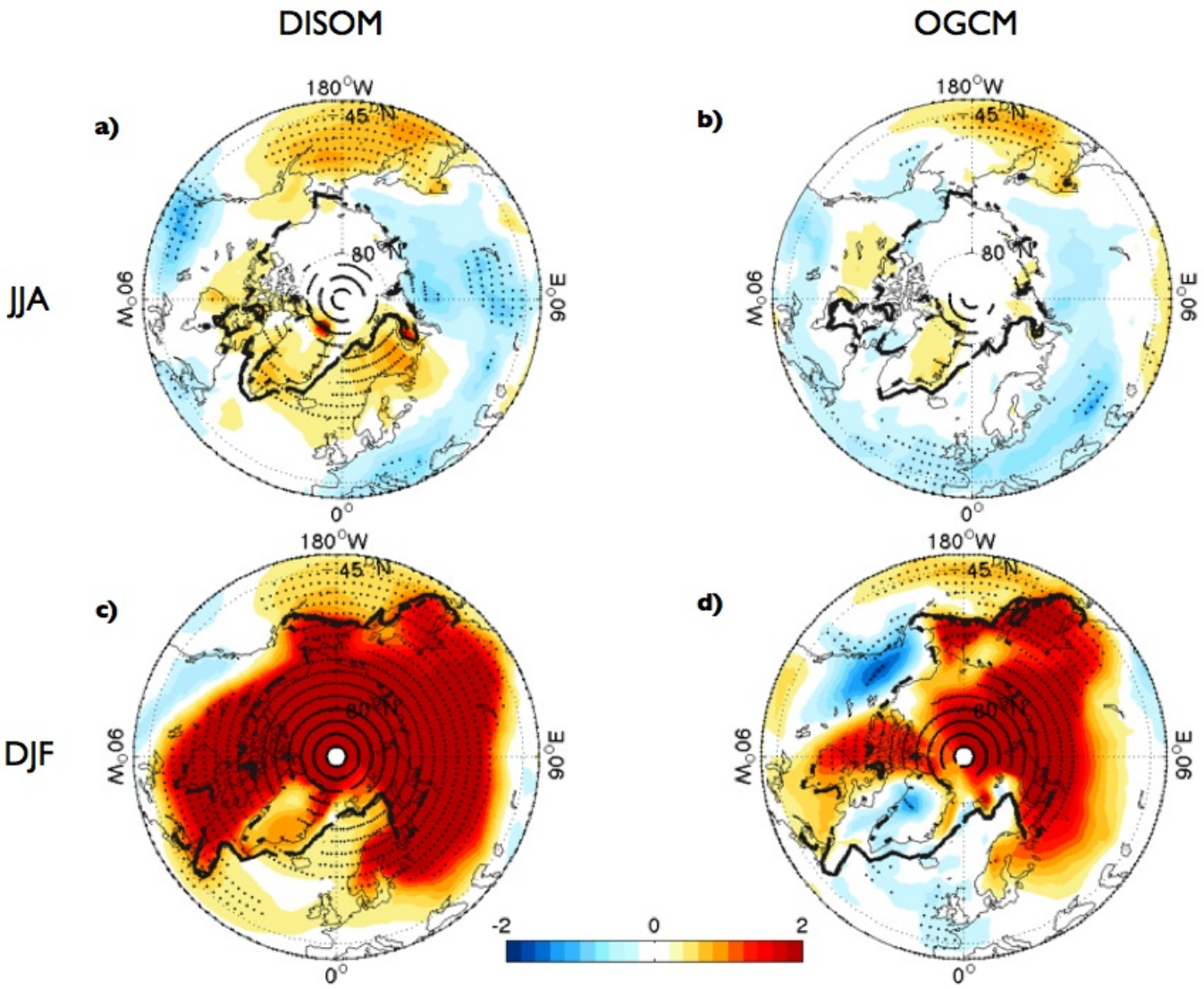

FIG. 6. The difference in mean JJA (a-b) and mean DJF (c-d) surface temperature (°C) between the *geoco2* runs and their corresponding *control* runs. Contours are 15% sea ice concentration in *control* (solid) and *geoco2* run (dashed). Results are for DISOM (a,c) and OGCM (b,d). Dots indicate regions of significant warming or cooling at the 95% level using the Student's t-test.

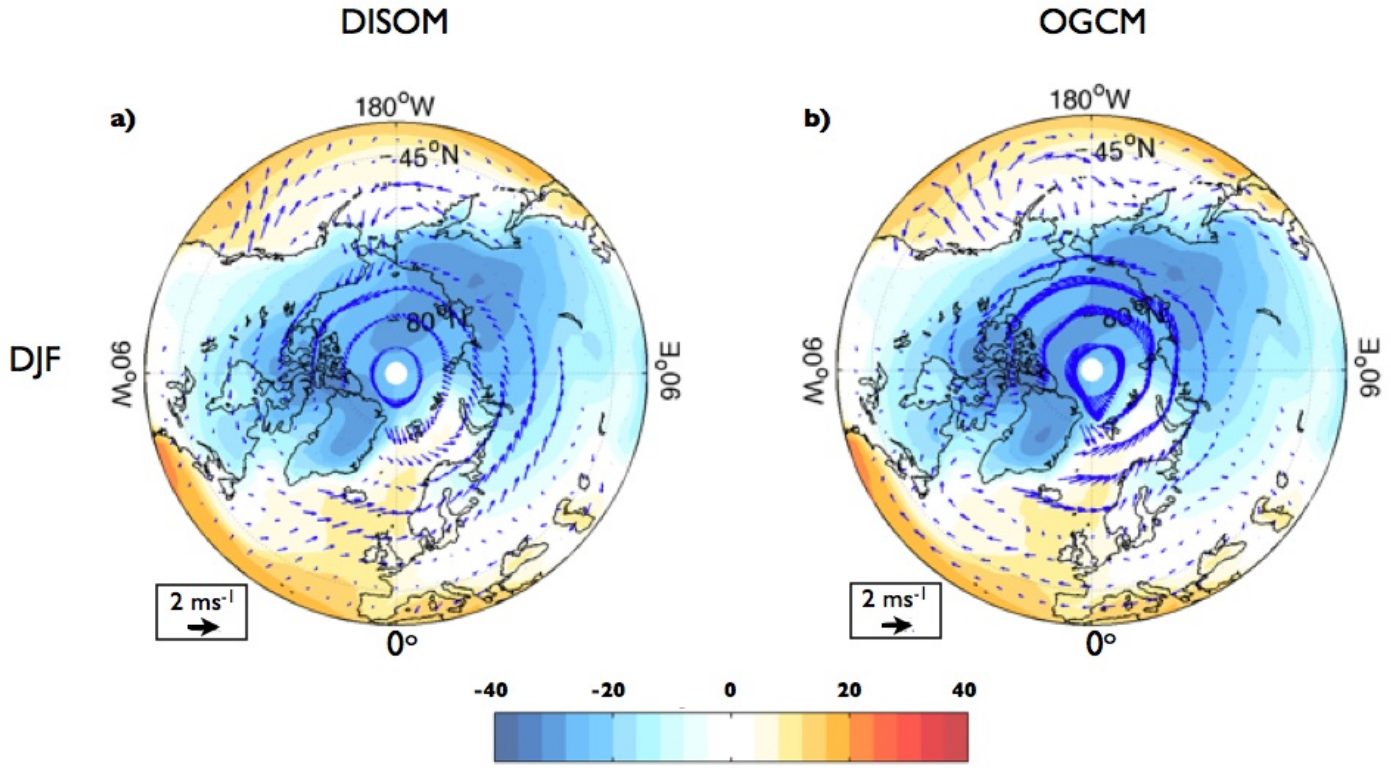

FIG. 7. The difference in mean DISOM (a) and OGCM (b) DJF 950 mb winds (m/s) between the *geoco2* runs and their corresponding *control* runs, and the climatological surface temperature in color (°C).

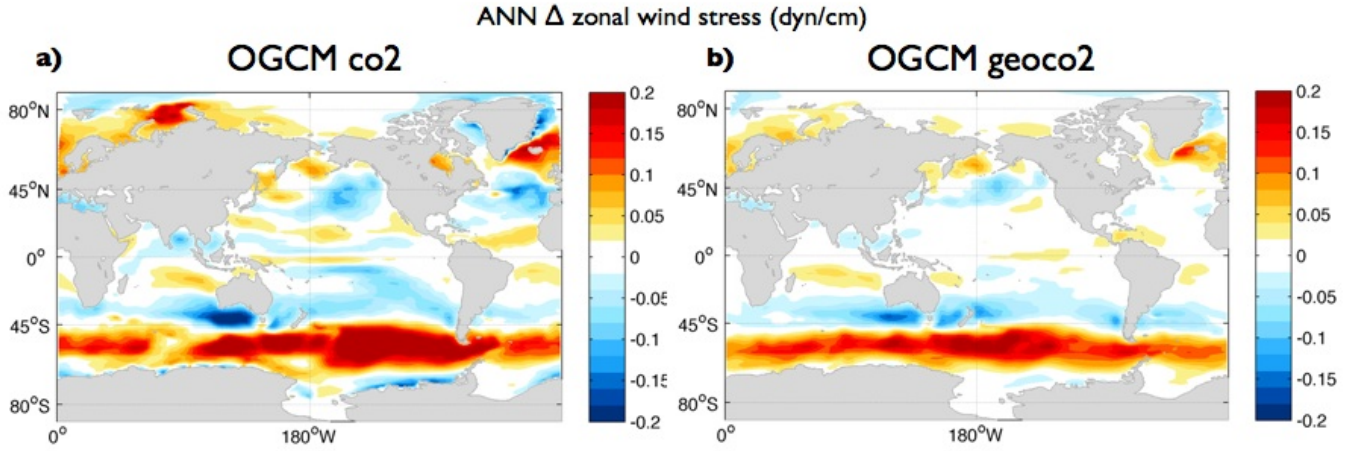

FIG. 8. Annual mean OGCM zonal wind stress difference (dyn/cm) between *co2* and *control* (a) and *geoco2* and *control* (b).

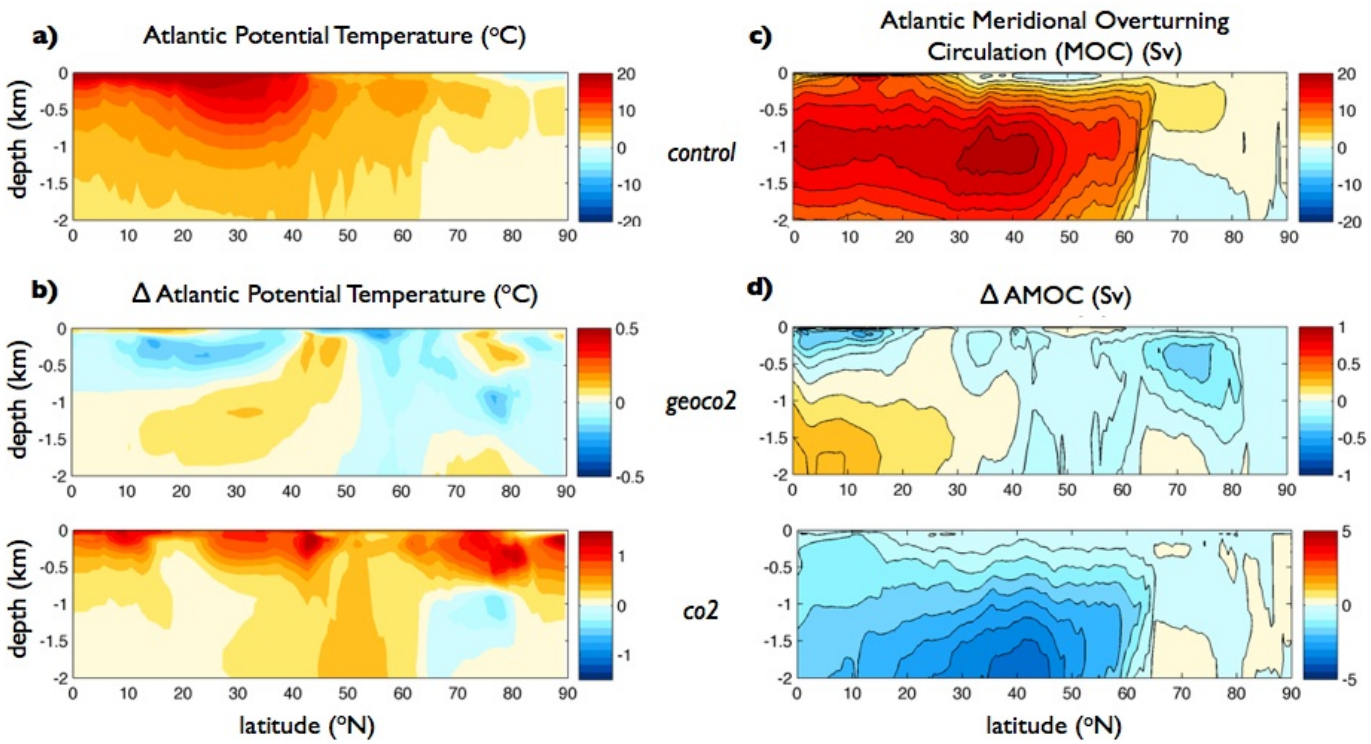

FIG. 9. Annual mean OGCM Atlantic Ocean zonal mean potential temperature (°C) for *control* (a) and perturbation experiment differences (b). Atlantic Ocean meridional overturning circulation (Sv) for *control* (c) and perturbation experiment differences (d). Note the smaller color scale for *geoco2* as compared to *co2*.

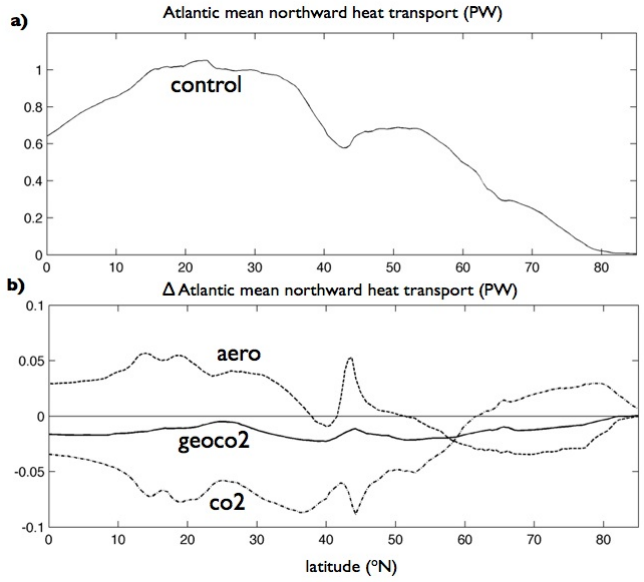

FIG. 10. Annual mean Atlantic Ocean northward heat transport in the *control* (a). Change in annual mean OGCM Atlantic Ocean northward heat transport (PW) for *geoco2* (solid), *co2* (dash-dot), and *aero* (dashed) (b).

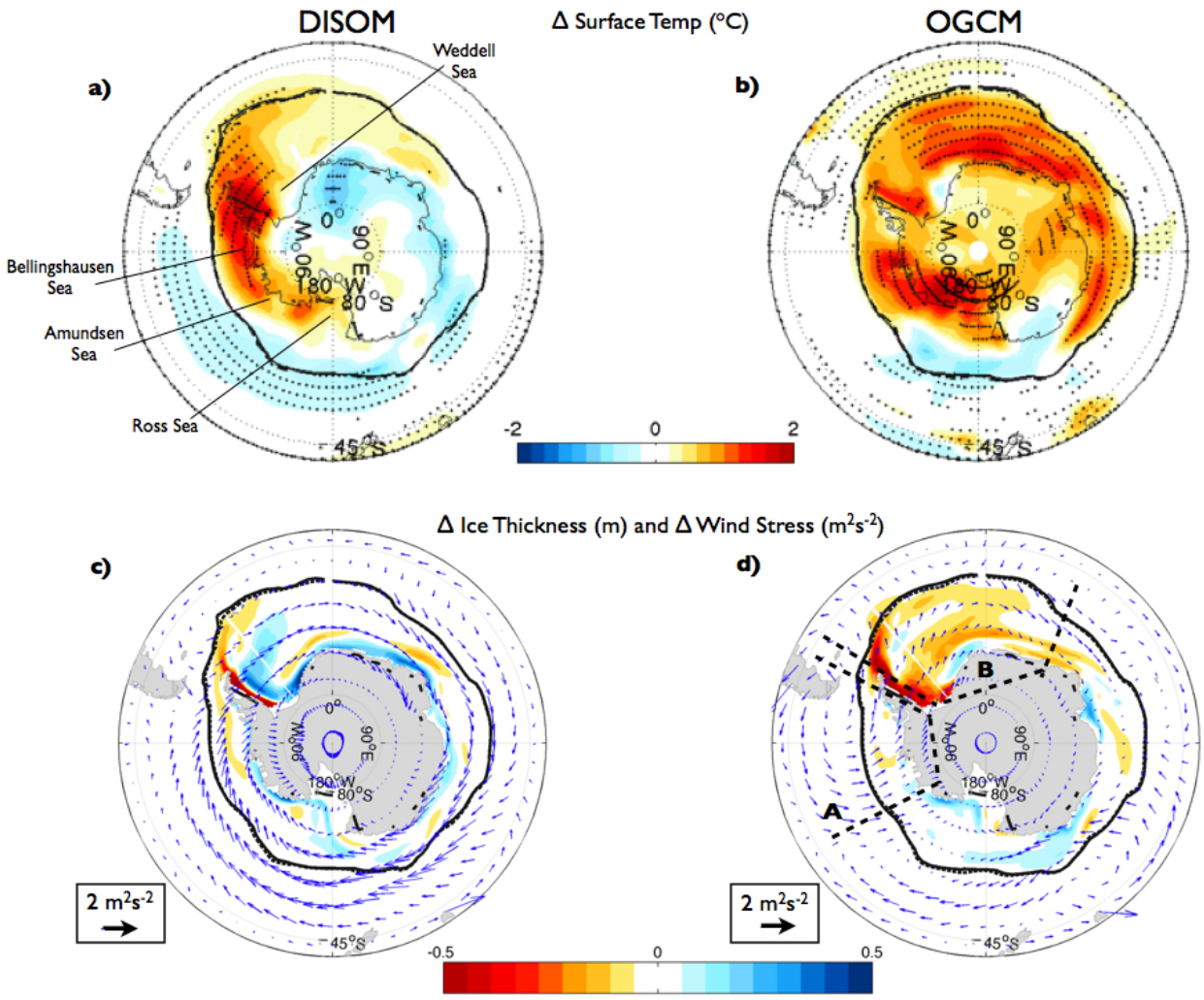

FIG. 11. (a-b) Mean JJA surface temperature change in *geoco2* minus *control* (color shading) and sea-ice extent defined as the 15% concentration contour in *control* (solid) and *geoco2* (dashed). Dots indicate regions of significant warming or cooling at the 95% level using the Student's t-test. Sea-ice extent in *geoco2* and control are nearly equal. (c-d) Mean JJA sea-ice thickness change in *geoco2* minus *control* (color shading) with sea-ice extent as in a-b. Vectors are differences in wind stress on the ocean. a,c) DISOM, b,d) OGCM.

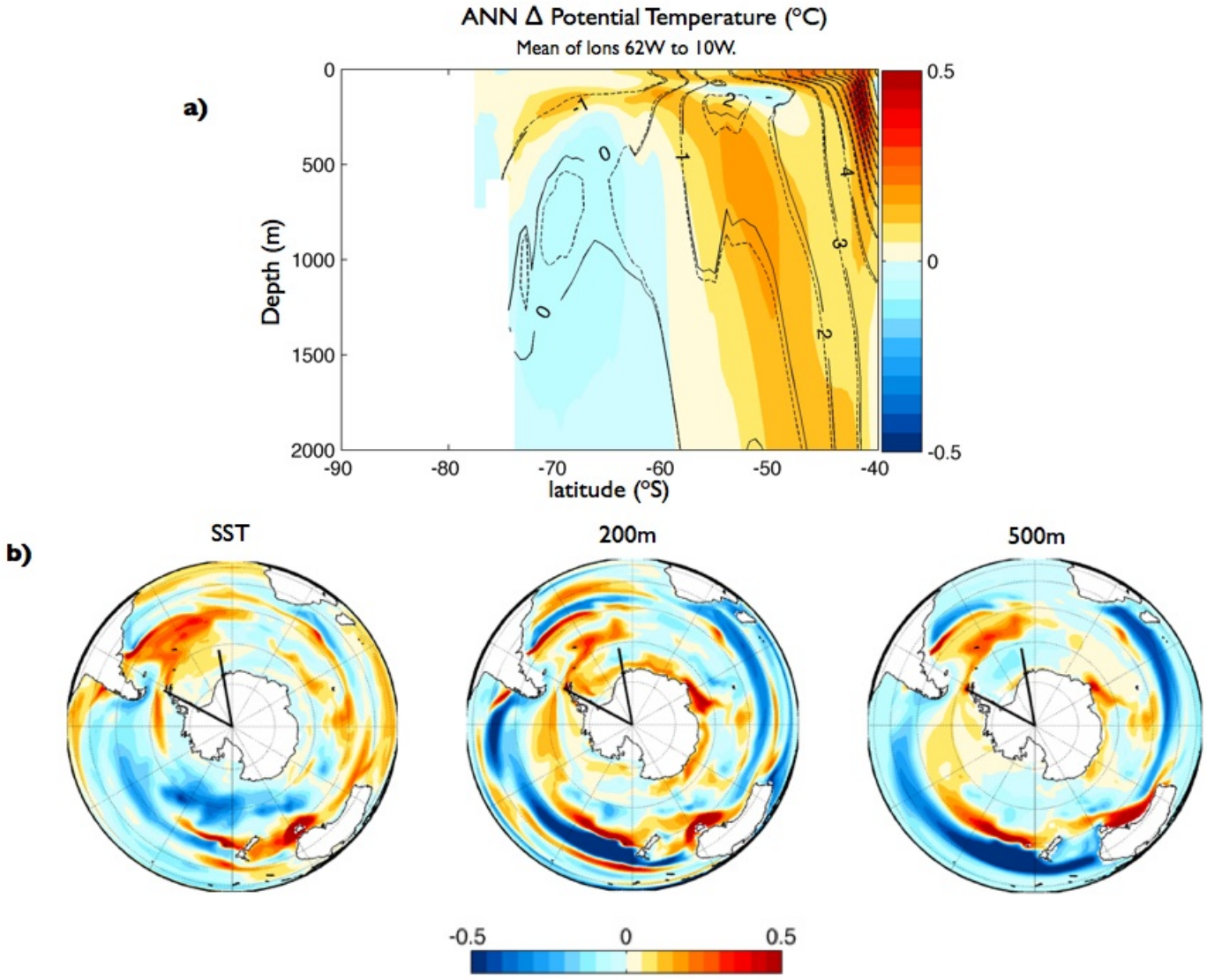

FIG. 12. Annual mean OGCM potential temperature difference (°C) between *geoco2* and *control* a) zonally averaged in the sector demarcated in (b) and b) shown at various depths. Contours are *control* (solid) and *geoco2* (dashed) potential temperatures in °C.

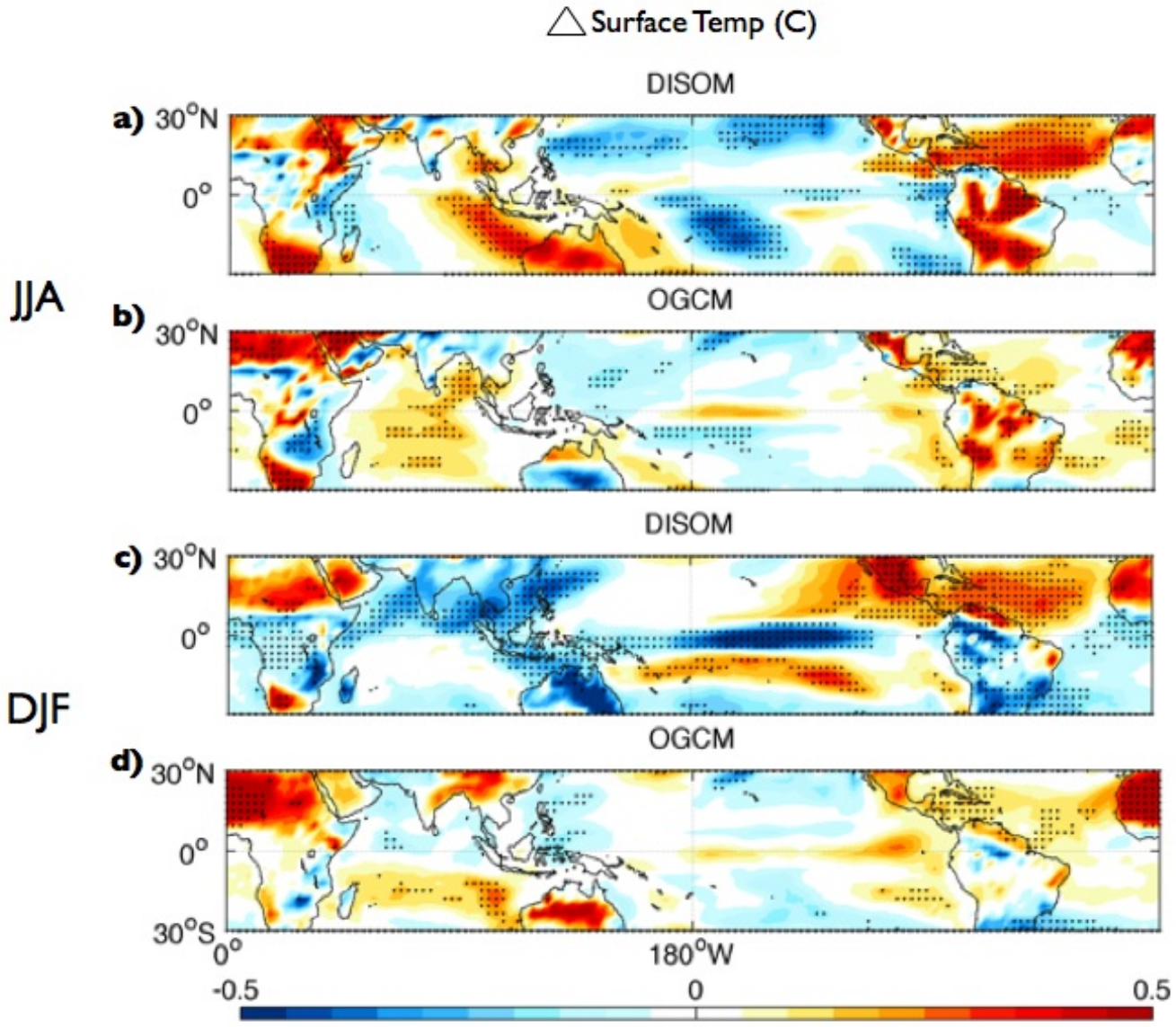

FIG. 13. The difference in mean JJA (a-b) and mean DJF (c-d) surface temperature (°C) between the *geoco2* runs and their corresponding *control* runs. a,c) DISOM, b,d) OGCM. Dots indicate regions of significant warming or cooling at the 95% level using the Student's t-test.

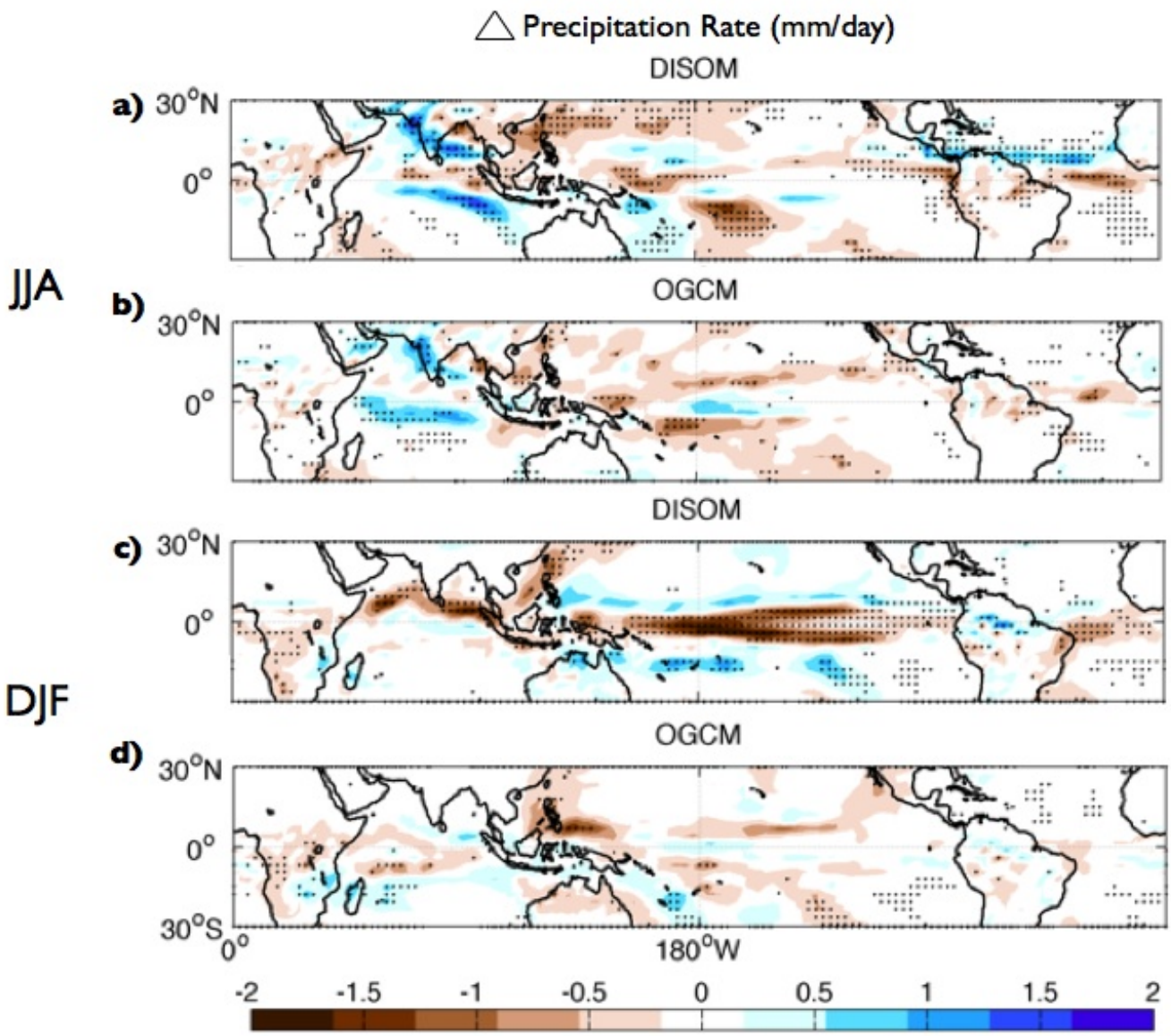

FIG. 14. The difference in mean JJA (a-b) and mean DJF (c-d) precipitation rate (mm/day) between the *geoco2* runs and their corresponding *control* runs. a,c) DISOM, b,d) OGCM. Dots indicate regions of significant precipitation change at the 95% level using the Student's t-test.

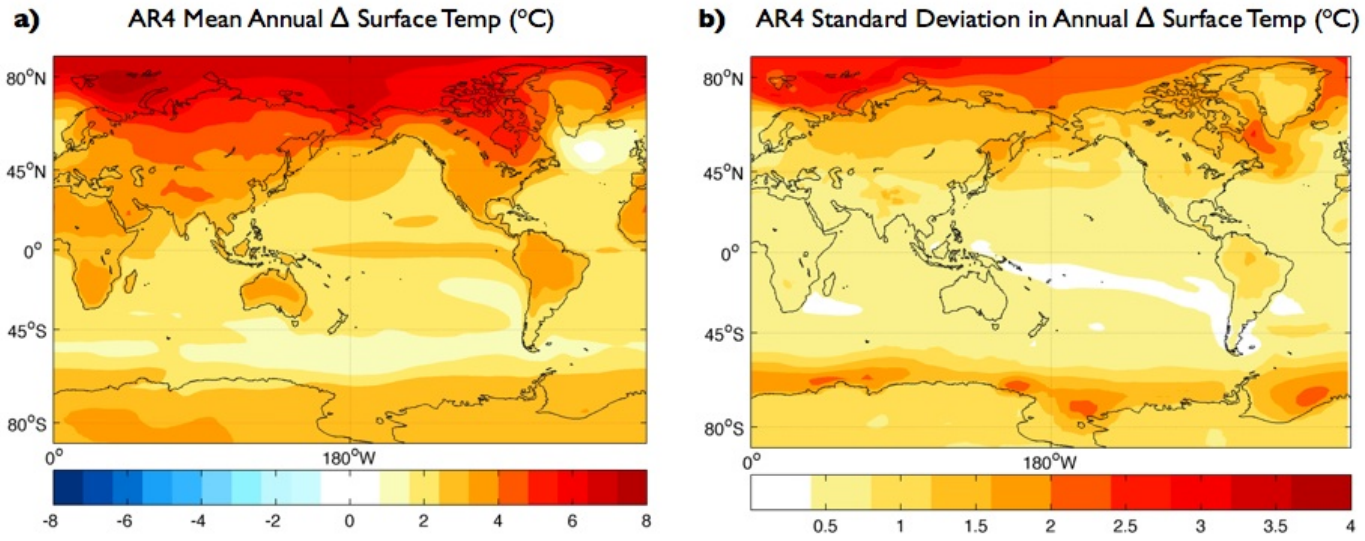

FIG. 15. The change in annual average surface temperature simulated by the CMIP3 models used in the latest IPCC Assessment Report. (a) The change over the 21st century (2080-2099 mean minus 1980-1999 mean), averaged across all the CMIP3 models. (b) The difference between the models, measured as the standard deviation of the simulated change from each model. Model output is from forcing using the A1B emissions scenario.